The Pennsylvania State University
APPLIED RESEARCH LABORATORY
P.O. Box 30
State College, PA 16804

ADAPTIVE FEEDFORWARD CONTROL OF STRUCTURAL INTENSITY IN A BEAM

by

A. E. Schwenk, S. D. Sommerfeldt, S. I. Hayek

Technical Report No. TR 92-05
October 1992

Supported by:
Space and Naval Warfare Systems Command

L.R. Hettche, Director
Applied Research Laboratory

Approved for public release; distribution unlimited

REPORT DOCUMENTATION PAGE

Form Approved
OMB No. 0704-0188

1. AGENCY USE ONLY (Leave blank)	2. REPORT DATE	3. REPORT TYPE AND DATES COVERED
	October 1992	

4. TITLE AND SUBTITLE

Adaptive Feedforward Control of Structural Intensity in a Beam

5. FUNDING NUMBERS

6. AUTHOR(S)

A. E. Schwenk, S. D. Sommerfeldt, S. I. Hayek

7. PERFORMING ORGANIZATION NAME(S) AND ADDRESS(ES)

The Applied Research Laboratory
P.O. Box 30
State College, PA 16804

8. PERFORMING ORGANIZATION REPORT NUMBER

TR-92-05

9. SPONSORING/MONITORING AGENCY NAME(S) AND ADDRESS(ES)

Space and Naval Warfare Systems Command
Department of the Navy
Washington, DC 20363-5000

10. SPONSORING/MONITORING AGENCY REPORT NUMBER

N00039-88-C-0051

11. SUPPLEMENTARY NOTES

12a. DISTRIBUTION/AVAILABILITY STATEMENT

Approved for Public Release. Distribution Unlimited.

12b. DISTRIBUTION CODE

13. ABSTRACT *(Maximum 200 words)*

This study examines methods for the adaptive control of structural vibration intensity in a beam. An algorithm, using finite difference techniques, is developed to calculate the total, instantaneous structural intensity. In addition, algorithms ased on the filtered-x least-mean-squares algorithm are developed to adaptively control the intensity. A real-time system identification algorithm is also described. To investigate the effectiveness of adaptive control of structural intensity, three control actuator and two error sensor configurations are used. Adaptive control is implemented at resonance and off-resonance frequencies, and the performance is evaluated by means of a separate accelerometer located in the farfield.

Experimental results demonstrate several trends. First, controlling the acceleration is considerably more effective with the error sensor located in the farfield than in the nearfield. Furthermore, controlling acceleration is more effective than controlling intensity, when the error sensors are in the farfield. Conversely, when the error sensors are in the nearfield, the attenuation achieved by controlling intensity is comparable to or greater than that achieved by controlling acceleration.

14. SUBJECT TERMS	15. NUMBER OF PAGES
adaptive control, structural vibration, intensity, beam, finite difference, x-least-mean-squares algorithm, real-time, resonance, off-resonance, feed forward	96
	16. PRICE CODE

17. SECURITY CLASSIFICATION OF REPORT	18. SECURITY CLASSIFICATION OF THIS PAGE	19. SECURITY CLASSIFICATION OF ABSTRACT	20. LIMITATION OF ABSTRACT
UNCLASSIFIED	UNCLASSIFIED	UNCLASSIFIED	

ABSTRACT

This study examines methods for the adaptive control of structural vibration intensity in a beam. An algorithm, using finite difference techniques, is developed to calculate the total, instantaneous structural intensity. In addition, algorithms based on the filtered-x least-mean-squares algorithm are developed to adaptively control the intensity. A real-time system identification algorithm is also described. To investigate the effectiveness of adaptive control of structural intensity, three control actuator and two error sensor configurations are used. Adaptive control is implemented at resonance and off-resonance frequencies and the performance is evaluated by means of a separate accelerometer located in the farfield.

Experimental results demonstrate several trends. First, controlling the acceleration is considerably more effective with the error sensor located in the farfield than in the nearfield. Furthermore, controlling acceleration is more effective than controlling intensity, when the error sensors are in the farfield. Conversely, when the error sensors are in the nearfield, the attenuation achieved by controlling intensity is comparable to or greater than that achieved by controlling acceleration.

TABLE OF CONTENTS

LIST OF FIGURES

LIST OF TABLES

Chapter 1

INTRODUCTION

Vibration control has always been an issue of concern for engineers. When one thinks of anything which is engineered, one generally encounters vibrations. Vibrations can be a problem for buildings that house rotating machinery, buildings that withstand wind loads, computers, and road surfaces. This study deals, specifically, with active control of structural vibration intensity in a beam and strives to deal with the larger problem of active vibration control.

Section 1.1 gives a brief history of adaptive control of vibrations. Section 1.2 gives a history of measurement and adaptive control of vibration intensity. Section 1.3 explains the work that was performed and the goals of the study. Section 1.4 details the structure of the thesis.

1.1 History of Adaptive Control

Adaptive control can be traced back as far as the 1950's when "Drenick and Shahbender borrowed the term 'adaptive' from biology where it describes the ability of an organism to adjust itself to its environment" [1,2]. In 1958, Anderson *et al.* [3] decided that an adaptive system must perform "a continuous measurement of system dynamic performance..., a continuous evaluation of the dynamic performance on the basis of some predetermined criterion," and "a continuous readjustment of system control parameters for 'optimum' operation..." Furthermore, in 1958, Grogin-

sky [4] decided that an adaptive system should outperform a conventional system by "allowing modifications of the control system while the system is in operation."

Non-adaptive active control of structural vibrations was studied in the 1950's, when Olson [5] generalized his "electronic sound absorber" to control vibrations. He called his device an "electronic vibration reducer," and he stated that it could "be used to isolate vibrating machines..." Adaptive control of structural vibrations was studied in the 1960's; Bonesho and Bollinger [6] described how to build a "self-optimizing vibration damper." The device used an analog control circuit to vary the damper's stiffness. The control criterion desired to have the "phase angle θ between motion of the damper mass m and main-system mass M ... [be] 90°..."

With recent developments in computer technology, most notably speed of processing, active control studies are becoming more prevalent. Studies in the 1980's investigated problems of vibrations from systems as simple as a beam to those as complex as a "flexible space telescope" [7]. Many control theories were and are being examined. Modal control and distributed-parameter control are replacing the single parameter control schemes of the 1950's [8,9,10].

In recent years much research has been performed generalizing the filtered-x algorithm developed by Widrow and Stearns [11: 288-294]. In 1990, Sommerfeldt and Tichy [12] developed an algorithm based on this filtered-x algorithm. Their control approach provided for real-time system identification and for multiple error, multiple output control. In 1991, Sommerfeldt [13] applied this algorithm, most notably, to the case of 4 error sensors and 4 control actuators. A similar algorithm

has also been developed to control sound fields; Sommerfeldt and Nashif [14], in 1992, used a filtered-x algorithm to investigate the differences between controlling the total acoustic energy density and controlling the squared pressure.

1.2 Vibration Intensity

This section describes the history of studies dealing with the measurement or control of vibration intensity. Section 1.2.1 gives a brief definition of terms used in this thesis. Section 1.2.2 gives a summary of previous studies.

1.2.1 Definition of Terms

The first term which needs to be defined is structural vibration intensity. Vibration intensity in a beam could also be referred to as mechanical power. Any power (electrical, mechanical, *etc.*) per unit area is referred to as intensity. Due to the constant area of a beam, having power flow in one dimension, the power and intensity vary by this constant area. Therefore, that which is referred to as intensity in this thesis is actually power.

The total, instantaneous intensity at a given point is a sum of two terms: the force intensity and the moment intensity. The force intensity is Fv--where F is the force, and v is the velocity--and the moment intensity is $M\Omega$--where M is the moment, and Ω is the angular velocity. The total, instantaneous intensity is represented as

$$\Pi = Fv + M\Omega. \tag{1.1}$$

The instantaneous intensity can be divided between active and reactive intensity. The active intensity is that which is propagating down, and out of, the beam (assuming there is any propagating intensity). The active intensity results from the force and velocity--and the moment and angular velocity--being in phase, and it has a time-averaged dc value. The reactive intensity is the intensity due to any standing waves in the beam. The time-averaged reactive intensity has a frequency twice that of the excitation vibration. Because the reactive intensity is periodic in time, it could be eliminated by taking a time average of the total intensity.

The time-averaged intensity is another quantity that will be studied. It can be expressed as

$$\langle \Pi \rangle_t = \frac{1}{2} Re\{Fv^*\} + \frac{1}{2} Re\{M\Omega^*\}. \tag{1.2}$$

1.2.2 Literature Concerning Vibration Intensity

There have been several studies of measurements of vibration intensity. In 1970, Noiseux [15] described a method for measuring the "power flow" in beams. He showed that, "at least for simple types of waves," the two terms of the intensity, force and moment, are equal in the far field, and he showed that the moment term could be measured using rotational accelerometers and strain gauges. In 1984, Pavic [16] described a method for measuring the intensity using an array of velocity

transducers. His scheme employed a four-point finite difference method to calculate the spatial derivatives needed to calculate structural intensity. Most recently, Suen [17] studied several finite difference methods that could be used to compute these spatial derivatives. He used a scanning laser vibrometer to measure the velocity along a beam, and then he calculated time-averaged intensity.

Fewer studies have investigated the control of vibration intensity. Redman-White *et al.* [18] investigated the "active control of flexural wave power flow" in 1987, and concluded "two closely spaced secondary force inputs can be used to absorb energy associated with the propagation of flexural waves in a uniform thin beam." In 1991, Pan and Hansen [19] performed an analysis of the control of power flow. Their study included an investigation into the effect of the orientation of the control actuator. Numerical analysis of a beam structure was performed with a variation of the angle of impact of the control force. Their results showed, notably, that, in order to control power flow effectively, the control force must be applied within a few degrees of the normal.

1.3 Goals of Thesis Research

The goal of this thesis is to develop an algorithm through which the total, instantaneous intensity can be measured and controlled. The study investigates methods for measuring the instantaneous intensity and develops an appropriate control algorithm. The study also deals with implementing the measurement and control algorithms and the problems associated with this implementation.

The ultimate goal of this study is to control the active intensity in a general structure. However, initially, it was decided to control the total intensity, both active and reactive. Also the structure used is a beam so as to limit the control study to one dimension.

1.4 Organization of the Thesis

Chapter 2 develops a more complete understanding of the intensity. The partial derivatives needed to calculate the intensity are explored, and the question of why one might want to control intensity is addressed. Chapter 3 investigates the terms necessary for calculating the intensity. It describes the finite difference schemes in both space and time. Also considered in Chapter 3 is the necessity of calibrating the accelerometer array, as well as additional calculation strategies that were investigated. Chapter 4 describes the development of the control algorithms. The projection algorithm, used for system identification is described first. The filtered-x algorithm, used for control, is described in general. Then the specific control schemes for implementing the filtered-x algorithm are developed. Chapter 5 gives a description of the experimental method. A description of the experimental hardware is given first. This is followed by a description of what data is collected and in what manner it is collected. Chapter 6 is a discussion of the experimental results. The validity of the intensity measurement is discussed, and the results of the various control strategies are also discussed. Chapter 7 deals with conclusions drawn from the study. Several recommendations for further research are also discussed.

Chapter 2

DESCRIPTION OF INTENSITY

This chapter develops a more complete understanding of the structural intensity. In Section 2.1, expressions for the total, instantaneous intensity and the time-averaged intensity are developed. Further, in Section 2.2, the theoretical advantage of controlling intensity is investigated.

2.1 Intensity Expressions

As defined in Section 1.2.1, the total, instantaneous intensity at any given point is the sum of two terms: the force term and the moment term.

The force term is equal to Fv. If E represents the Young's modulus, and I represents the moment of inertia of the cross section, then the force can be represented, in terms of the transverse displacement $\xi(x,t)$, as

$$F=EI\frac{\partial^3\xi}{\partial x^3}. \tag{2.1}$$

The velocity, v, can be expressed as

$$v=\frac{\partial\xi}{\partial t}. \tag{2.2}$$

The moment term is equal to $M\Omega$. The moment can be represented by

$$M=-EI\frac{\partial^2\xi}{\partial x^2}. \tag{2.3}$$

The angular velocity, Ω, can be expressed as

$$\Omega=\frac{\partial^2\xi}{\partial t\partial x}. \tag{2.4}$$

The total, instantaneous intensity, therefore, can be expressed as

$$\Pi=EI\frac{\partial^3\xi}{\partial x^3}\frac{\partial\xi}{\partial t}-EI\frac{\partial^2\xi}{\partial x^2}\frac{\partial^2\xi}{\partial t\partial x}. \tag{2.5}$$

It follows that the time-averaged intensity expression given in Eq. (1.2) can be represented by

$$\langle\Pi\rangle_t=\frac{1}{2}Re\left[EI\frac{\partial^3\xi}{\partial x^3}\left[\frac{\partial\xi}{\partial t}\right]^*\right]-\frac{1}{2}Re\left[EI\frac{\partial^2\xi}{\partial x^2}\left[\frac{\partial^2\xi}{\partial t\partial x}\right]^*\right]. \tag{2.6}$$

2.2 Theoretical Advantage of Controlling Intensity

The following developments were performed by Dr. S.D. Sommerfeldt (1991) in an Acoustics class at the Pennsylvania State University.

Consider the problem of controlling the vibration in an infinite beam, as shown in Figure 2.1. It is assumed that the beam is excited by a driving force, $F_p e^{j\omega t}$, located at $x=0$, and a complex control force,

$$\tilde{F}_c e^{j\omega t} = (F_{c,R} + jF_{c,I}) e^{j\omega t}, \tag{2.7}$$

located at $x=L$. F_n is taken to be real with no loss in generality. The region of interest is taken to be $x \geq L$. The two solutions considered are the control of time-averaged intensity and the control of the transverse acceleration at a point $x \geq L$.

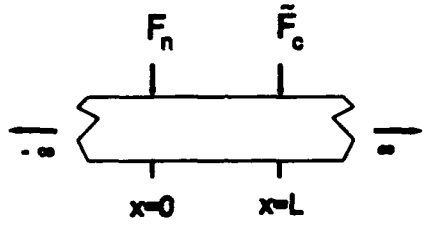

Figure 2.1 Diagram of Infinite Beam with Control.

The control of time-averaged intensity is considered first. The displacement of the beam can be represented by

$$\begin{aligned} \xi(x,t) &= \frac{j}{4EIk^3}\left[-F_n e^{-jkx} + jF_n e^{-kx} - \tilde{F}_c e^{-jk(L-x)} + j\tilde{F}_c e^{-k(L-x)}\right] e^{j\omega t}; \\ &\qquad\qquad 0 \leq x \leq L \\ &= \frac{j}{4EIk^3}\left[-F_n e^{-jkx} + jF_n e^{-kx} - \tilde{F}_c e^{-jk(x-L)} + j\tilde{F}_c e^{-k(x-L)}\right] e^{j\omega t}; \\ &\qquad\qquad x \geq L \ , \end{aligned} \tag{2.8}$$

where $j=\sqrt{-1}$, and k is the flexural wavenumber. Internal structural losses have been ignored in this formulation. From Eq. (1.2), the time-averaged intensity at any point can be expressed as

$$\langle \Pi \rangle_t = \frac{1}{2} Re\{F v^*\} + \frac{1}{2} Re\{M \Omega^*\}. \tag{2.9}$$

In order to calculate the control solution, one must first determine the intensity expression for $x \geq L$. Performing the necessary partial differentiation results in expressions for F, v, M, and Ω:

$$F = \frac{1}{4}\left[F_n e^{-jkx} + F_n e^{-kx} + \tilde{F}_c e^{-jk(x-L)} + \tilde{F}_c e^{-k(x-L)}\right] e^{j\omega t}, \tag{2.10}$$

$$v = \frac{-\omega}{4EIk^3}\left[-F_n e^{-jkx} + jF_n e^{-kx} - \tilde{F}_c e^{-jk(x-L)} + j\tilde{F}_c e^{-k(x-L)}\right] e^{j\omega t}, \tag{2.11}$$

$$M = \frac{-j}{4k}\left[F_n e^{-jkx} + jF_n e^{-kx} + \tilde{F}_c e^{-jk(x-L)} + j\tilde{F}_c e^{-k(x-L)}\right] e^{j\omega t}, \tag{2.12}$$

and

$$\Omega = \frac{-j\omega}{4EIk^2}\left[F_n e^{-jkx} - F_n e^{-kx} + \tilde{F}_c e^{-jk(x-L)} - \tilde{F}_c e^{-k(x-L)}\right] e^{j\omega t}. \tag{2.13}$$

Substituting these expressions into Eq. (2.9) gives

$$\langle \Pi \rangle_t = \frac{\omega}{32EIk^3}\left[2F_n^2 + 4F_n F_{c,R}\cos(kL) - 4F_n F_{c,I}\sin(kL) + 2\bar{F}_c^2\right]. \tag{2.14}$$

In order to determine the desired control, the time-averaged intensity is minimized with respect to the control force. Because the control force is complex, this involves two partial differentiations:

$$\frac{\partial \langle \Pi \rangle_t}{\partial F_{c,R}} = 0 \tag{2.15}$$

and

$$\frac{\partial \langle \Pi \rangle_t}{\partial F_{c,I}} = 0. \tag{2.16}$$

The solution of the two equations (2.15) and (2.16) yields the requisite control force components:

$$F_{c,R} = -F_n \cos(kL) \tag{2.17}$$

and

$$F_{c,I} = F_n \sin(kL). \tag{2.18}$$

Using Euler's relation, these can be combined to yield

$$\bar{F}_c = -F_n e^{-i(kL)}. \tag{2.19}$$

Substituting this into Eq. (2.14) gives

$$\langle \Pi \rangle_t = 0; x \geq L \tag{2.20}$$

Further, substituting Eq. (2.19) into Eq. (2.8) yields

$$\xi(x,t) = -\frac{F_n e^{-kx}}{4EIk^3}\left[1 - e^{kL} e^{-jkL}\right] e^{j\omega t}; x \geq L; \tag{2.21}$$

that is, $\xi(x,t)$ decays exponentially to 0 for $x>L$. These relations are true regardless of the location of the intensity measurement used for control.

An analogous development is given for the control of the acceleration at a single point. Again considering the infinite beam configuration shown in Figure 2.1, the acceleration for $x \geq L$ can be obtained from Eq. (2.8) as

$$a(x,t) = \frac{-j\omega^2}{4EIk^3}\left[-F_n e^{-jkx} + jF_n e^{-kx} - \tilde{F}_c e^{-jk(x-L)} + j\tilde{F}_c e^{-k(x-L)}\right] e^{j\omega t}. \tag{2.22}$$

This acceleration is set equal to 0 at some location $x_0>L$:

$$a(x_0,t) \propto -F_n e^{-jkx_0} + jF_n e^{-kx_0} - \tilde{F}_c e^{-jk(x_0-L)} + j\tilde{F}_c e^{-k(x_0-L)} = 0. \tag{2.23}$$

Solving for $\tilde{F}_c$ yields

$$\tilde{F}_c = -\frac{e^{-jkx_0} - je^{-kx_0}}{e^{-jk(x_0-L)} - je^{-k(x_0-L)}} F_n. \tag{2.24}$$

Substituting this into the expression for displacement yields an expression which, in general, is not equal to 0 for $x \geq L$. If, however, the point, x_0, is far removed from L, such that $kx_0>>1$ and $k(x_0-L)>>1$, the control force reduces to

$$\tilde{F}_c = -e^{-jkL} F_n. \tag{2.25}$$

This is the same control force that is found in Eq. (2.19) for the case of controlling the time-averaged intensity at any point $x \geq L$. As is the case with intensity control, substituting this control force into the expression for displacement at $x \geq L$ results in $\xi(x,t)$ decaying exponentially to 0 for $x > L$.

The problem with controlling acceleration is that the error sensor must be located far (relative to a wavelength) from the source or any boundaries or discontinuities. In any but the simplest structures, this is difficult if not impossible.

The theoretical advantage of controlling intensity, time-averaged at least, is that the error sensor can be located as close to the control source as geometrical constraints allow. With complicated structures, such as frames, this suggests that the vibration could be confined to the region between the vibration source and the control source--entirely within the first spar.

Chapter 3

CALCULATION OF INTENSITY

Many different ways of determining structural intensity have been studied in the past few years. Sensors ranging from accelerometers, strain gauges, and force gauges to laser velocimeters and vibrometers have been employed in this endeavor. In this study, accelerometers alone are considered for the measurement of total, instantaneous intensity. This does not, however, determine the method for utilizing these point acceleration measurements to calculate the structural intensity.

An array of 5 accelerometers, positioned on the top of the beam is used. The spacing between accelerometers is constant. As is shown in Figure 3.1, the accelerometers are arrayed in one dimension, and the accelerometer positions are numbered sequentially. The acceleration signal at position i at time t is referred to as $a_{i,t}$.

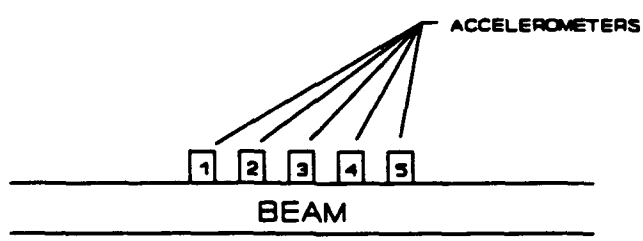

Figure 3.1 Accelerometer Array Positioning.

In Eq. (2.5) the total, instantaneous intensity is expressed as a function of the transverse displacement. If a time-harmonic vibration, with frequency ω_0, is assumed, then the displacement, as a function of the transverse acceleration, can be represented by

$$\xi(x,t)=-\frac{1}{\omega_0^2}a(x,t). \tag{3.1}$$

With this expression for ξ, the total, instantaneous intensity at position 3 is expressed as

$$\Pi_3=EI\left(\frac{-1}{\omega_0^2}\frac{\partial^3 a_3}{\partial x^3}\right)\left(\frac{-1}{\omega_0^2}\frac{\partial a_3}{\partial t}\right)-EI\left(\frac{-1}{\omega_0^2}\frac{\partial^2 a_3}{\partial x^2}\right)\left(\frac{-1}{\omega_0^2}\frac{\partial^2 a_3}{\partial t\partial x}\right). \tag{3.2}$$

In order to calculate this expression for structural intensity, the various time and space derivatives of the acceleration at position 3 must be calculated.

This chapter describes the various calculation tools used in this study to determine the necessary derivatives and the resulting structural intensity. The chapter also describes some additional strategies that were studied and discarded. Section 3.1 describes the technique used to calculate the time differentials of the accelerations; Section 3.2 describes the technique used to calculate the space differentials of both the accelerations and the previously calculated time differentials. Section 3.2 also shows the conclusion of the intensity calculations. Section 3.3 describes the importance and the method of calibrating the accelerometers in the intensity array.

Section 3.4 describes several other techniques studied for dealing with time differentials.

3.1 Time Differentials

The technique used to calculate the time differentials of the accelerations (these time differentials will be used to determine the velocity and angular velocity terms) is a backward finite difference technique. The particular finite difference scheme chosen is that with error on the order of τ^2, where τ is the time increment between samples. The scheme is chosen to be a backward finite difference scheme because the accelerations are known only up to and including the time at which the time derivatives are desired. The scheme is chosen to be that with an error on the order of τ^2 because the error at this step must be minimized to keep the error low in the ensuing spatial derivative calculations.

The velocity term, v, at time t is obtained by implementation of the backward finite difference formula on acceleration a_3 at time t, that is $a_{3,t}$:

$$\frac{\partial a_{3,t}}{\partial t} = \frac{3a_{3,t} - 4a_{3,t-1} + a_{3,t-2}}{2\tau} + O(\tau^2). \qquad (3.3)$$

In order to determine the angular acceleration term, Ω, at time t, it is necessary to calculate the time differentials at positions 2 and 4

$$\frac{\partial a_{2,t}}{\partial t}=\frac{3a_{2,t}-4a_{2,t-1}+a_{2,t-2}}{2\tau}+O(\tau^2) \tag{3.4}$$

and

$$\frac{\partial a_{4,t}}{\partial t}=\frac{3a_{4,t}-4a_{4,t-1}+a_{4,t-2}}{2\tau}+O(\tau^2). \tag{3.5}$$

3.2 Space differentials

Space differentials are used to calculate the force, moment, and angular velocity terms. The technique used to calculate the space differentials is a central finite difference scheme. The particular scheme has error on the order of Δ^2, where Δ is the spacing between accelerometers. This scheme was chosen because Suen [17] has shown, that of the schemes that he studied, this "second order scheme ... caused the least error in computing the structural intensity."

The force term, F, requires the calculation of the third spatial derivative of the acceleration at point 3. (Note: The lack of a time subscript implies the term is at time t.) Using a central difference formula, this spatial derivative can be obtained as

$$\frac{\partial^3 a_3}{\partial x^3}=\frac{-a_1+2a_2-2a_4+a_5}{2\Delta^3}+O(\Delta^2). \tag{3.6}$$

The moment term, M, requires the calculation of the second spatial derivative of the acceleration at point 3, which can be obtained as

$$\frac{\partial^2 a_3}{\partial x^2}=\frac{a_2-2a_3+a_4}{\Delta^2}+O(\Delta^2). \tag{3.7}$$

The angular velocity term, Ω, requires the calculation of the first spatial derivative of the time differential of a_3. This scheme employs the time derivatives of $a_{2,t}$ and $a_{4,t}$ shown previously in Eqs. (3.4) and (3.5). This spatial derivative is obtained as

$$\frac{\partial^2 a_3}{\partial t \partial x}=\frac{-\frac{\partial a_2}{\partial t}+\frac{\partial a_4}{\partial t}}{2\Delta}+O(\Delta^2). \tag{3.8}$$

Assuming the above partial derivatives have been calculated, the total, instantaneous intensity can be calculated. Due to the fact that the operations have been performed on accelerations, and not displacements, a double integration must be performed. This double integration is achieved by multiplying each term by $-1/\omega_0^2$, where ω_0 is the frequency of excitation. (This implies that this method of calculating intensity is only valid for single frequencies, with the frequency of excitation known.) Thus the quantities needed to determine the structural intensity can be summarized:

$$F_3=EI\frac{\partial^3 \xi_3}{\partial x^3}=-\frac{EI}{\omega_0^2}\frac{\partial^3 a_3}{\partial x^3}, \tag{3.9}$$

$$v_3=\frac{\partial \xi_3}{\partial t}=-\frac{1}{\omega_0^2}\frac{\partial a_3}{\partial t}, \tag{3.10}$$

$$M_3 = -EI\frac{\partial^2 \xi_3}{\partial x^2} = \frac{EI}{\omega_0^2}\frac{\partial^2 a_3}{\partial x^2}, \tag{3.11}$$

and

$$\Omega_3 = \frac{\partial^2 \xi_3}{\partial t \partial x} = -\frac{1}{\omega_0^2}\frac{\partial^2 a_3}{\partial t \partial x}. \tag{3.12}$$

Because F and v are multiplied and M and Ω are multiplied, the resulting factor is $1/\omega_0^4$. Realizing that both F and M have factors of EI, the resulting expression for total, instantaneous intensity is calculated as

$$\Pi_3 = \frac{EI}{\omega_0^4}\left[\frac{\partial^3 a_3}{\partial x^3}\frac{\partial a_3}{\partial t} - \frac{\partial^2 a_3}{\partial x^2}\frac{\partial^2 a_3}{\partial t \partial x}\right]. \tag{3.13}$$

3.3 Calibration of the Accelerometers

When applying spatial finite differences, it is important to calibrate the accelerometers relative to a reference accelerometer. The accelerometers do not necessarily have to be calibrated absolutely because the adaptive nature of the control algorithm will correct for any uniform bias across the array.

Due to the single frequency nature of the excitation, the accelerometers are calibrated at specific frequencies of interest. To do this, two accelerometers (one reference accelerometer and one to be calibrated) are excited with an impulse and the

response of each recorded. Then a ratio of the magnitude of the responses is taken at various frequencies. For example, if the reference accelerometer is referred to as *R*, then the calibration coefficient of accelerometer *A* at 300 Hz is equal to the magnitude of the response of *R* at 300 Hz divided by the magnitude of the response of *A* at 300 Hz.

3.4 Additional Schemes Studied

This study investigated other strategies for dealing with the time dependence in the calculation of intensity. These dealt with the problem differently. The spatial finite difference scheme was used, but instead of taking time differentials and then double integrating with $-1/\omega_0^2$, it was attempted to perform a numerical integration of the accelerations. A single integration of a_2, a_3, and a_4 would be necessary to get the velocity term and to get the velocities needed to calculate the angular velocity term. Double integration of all five accelerations would be needed to get the displacements needed to calculate the force and moment terms. Several numerical integration techniques were studied, including various Adams-Moulton schemes and schemes adapted from digital filter integrators [20].

By means of simulating the integration techniques, it was found that all of these additional schemes gave intolerable error. The most common type of error was a linearly increasing error. This error quite often started out small and grew slowly. However, the goal is to run the control indefinitely, and any continuing growth in the error is deemed intolerable. Another consideration with these numerical integration

techniques is picking proper initial conditions. The question arises as to what a valid assumption for the initial velocities and displacements is. This question was not resolved due to the fact that the techniques were unacceptable. One advantage with differentiation is that one does not need to make any assumption about the initial conditions, although differentiation does introduce high-frequency noise into the results.

Chapter 4

DESCRIPTION OF CONTROL ALGORITHMS

Having decided upon a means of calculating the total, instantaneous intensity, the various means of controlling this intensity are investigated. The algorithms used for the control system are the projection algorithm, which is used for system identification, and the filtered-x least-mean-squares algorithm, which is used to update the control filters. These algorithms are described in this chapter. The system identification algorithm is described first, in Section 4.1, because it is necessary to have these filters converge to their stable values before the control filters can converge to their stable values. Section 4.2 describes the filtered-x least-mean-squares algorithm.

4.1 System Identification

The algorithm used for system identification is called the projection algorithm or the normalized least-mean-squares (NLMS) algorithm. In this application of the algorithm, there is assumed to be one error sensor, measuring the error signal, $\varepsilon(m)$, where m is the discrete time index. The system identification algorithm attempts to find functional transfer functions correlating the input trace and the control signals to this error signal. The error signal can be considered as consisting of two parts: the signal which is present in the absence of control (*i.e.* that which one is trying to control) and that which arises due to control forces driving the system. In the early

literature [11: 9-10] the element of the error signal one is trying to control is referred to as the "desired signal," $d(m)$; apparently, because this is the signal one "desires" to match with the adaptive system. If one assumes that N control actuators are used, the element of the error signal which arises due to control forces added to the system can be approximated by passing the control outputs, $y_n(m)$, through corresponding transfer functions, $H_n(m)$. The transfer function from the n^{th} control actuator to the error signal is represented by a linear Finite Impulse Response (FIR) filter vector with K coefficients, or taps,

$$H_n^T(m) = [h_{n0}(m)\, h_{n1}(m) \cdots h_{n(K-1)}(m)]. \tag{4.1}$$

The time train of y_n necessary to implement this FIR filter also has K terms and is represented by

$$Y_n^T(m) = [y_n(m)\, y_n(m-1) \cdots y_n(m-K+1)]. \tag{4.2}$$

The element of the error signal that arises due to the n^{th} control actuator can be represented by a convolution sum

$$e_n(m) = \sum_{k=0}^{K-1} h_{nk}(m) y_n(m-k). \tag{4.3}$$

In vector notation, this is expressed as

$$e_n(m) = H_n^T(m) Y_n(m). \tag{4.4}$$

For notational convenience, a composite control path transfer function vector can be represented as a concatenation of the N transfer function vectors,

$$H^T(m) = \left[H_1^T \| H_2^T \| \cdots \| H_N^T\right] = \left[h_{10} \cdots h_{1(K-1)} \| h_{20} \cdots h_{2(K-1)} \| \cdots \| h_{N0} \cdots h_{N(K-1)}\right]. \quad (4.5)$$

Likewise, a composite control output vector can be formed as a concatenation of the N time trains,

$$Y^T(m) = \left[Y_1^T(m) \| Y_2^T(m) \| \cdots \| Y_N^T(m)\right]. \quad (4.6)$$

Using this notation, the total error signal can be expressed as

$$e(m) = d(m) + Y^T(m)H(m). \quad (4.7)$$

However, in implementing the projection algorithm, a necessary condition to achieve convergence is that the entire error signal be approximated. A necessary condition for the control algorithm to provide attenuation is that the desired signal, $d(m)$, be correlated with the input trace. This relationship can be modelled through the implementation of an additional transfer function filter

$$d(m) = \sum_{k=0}^{K-1} h_{(N+1)k}(m)x(m-k). \quad (4.8)$$

If the $x(m-k)$ vector is concatenated with $Y^T(m)$, one obtains the data vector,

$$\Phi^T(m) = \left[Y_1^T(m) \| \cdots \| Y_N^T(m) \| x(m)x(m-1) \cdots x(m-K+1)\right]. \quad (4.9)$$

Likewise, if the $H^T_{(N+1)}(m)$ vector is concatenated with $H^T(m)$, one obtains the coefficient vector,

$$\Theta^T(m) = \left[H_1^T \| \cdots \| H_N^T \| h_{(N+1)0} \cdots h_{(N+1)(K-1)}\right]. \tag{4.10}$$

Now the total error signal used by the system identification algorithm can be expressed as

$$\varepsilon(m) = \Theta^T(m)\Phi(m) \tag{4.11}$$

[21: 70-75]. One can calculate $y_n(m)$, and one can measure $\varepsilon(m)$ and $x(m)$. With this knowledge, the Projection (or NLMS) Algorithm can be employed to converge upon values for $\Theta(m)$. If the estimated value of $\Theta(m)$ is represented by $\hat{\Theta}(m)$, then this estimate is updated according to the Projection Algorithm,

$$\hat{\Theta}(m+1) = \hat{\Theta}(m) + \frac{a\Phi(m)}{b+\Phi^T(m)\Phi(m)}\left[\varepsilon(m) - \hat{\Theta}^T(m)\Phi(m)\right], \tag{4.12}$$

where $\hat{\Theta}(m+1)$ is the updated transfer function estimate, a is a convergence parameter--chosen to be $0<a<2$ for stability--and b is a small, positive constant used to ensure that there is no division by zero [22: 50-54].

4.2 Control

The algorithm used for the control filter update is called the filtered-x least-mean-squares (filtered-x) algorithm; it is similar to one developed by Widrow and Stearns [11: 288-294]. This algorithm is used to determine the N control signals, $y_n(m)$, which minimize a mean-squared-error signal. The control signals are obtained by passing the system input, $x(m)$, through the control filters, $W_n(m)$. These control filters are each represented by a FIR filter vector with I taps

$$W_n^T(m) = \left[w_{n0}(m)\, w_{n1}(m) \cdots w_{n(I-1)}(m)\right]. \tag{4.13}$$

The time train of the input signal, $x(m)$, necessary to implement this FIR filter also has I terms and is represented by

$$X^T(m) = \left[x(m)\, x(m-1) \cdots x(m-I+1)\right]. \tag{4.14}$$

A convolution sum of these two signals gives the n^{th} control output

$$y_n(m) = \sum_{i=0}^{I-1} w_{ni}(m) x(m-i) = W_n^T X, \tag{4.15}$$

where $w_{ni}(m)$ are the n^{th} control filter coefficients at time m, $y_n(m)$ is the n^{th} control filter output at time m, and $x(m-i)$ is the input to the control filters at time m-i. A composite control filter vector can be formed as the concatenation of the N control filter vectors:

$$W^T(m) = \left[W_1^T(m) \| W_2^T(m) \| \cdots \| W_N^T(m)\right]. \tag{4.16}$$

The optimal solution for the control filter vector is taken to be the solution which minimizes the mean-squared-error signal. The filtered-x algorithm is a steepest descent algorithm which is based on the concept of updating the control filter coefficients according to the negative of the gradient with respect to the filter coefficients of the mean-squared error, so that the control filters converge to the optimal solution in an iterative manner. The mean-squared error is approximated by the instantaneous squared error, $e^2(m)$. This error signal, $e(m)$, is not necessarily the same

as the error signal used in the system identification algorithm, $\varepsilon(m)$. The update equation is expressed as

$$W(m+1)=W(m)-\mu_0\nabla_W e^2(m). \tag{4.17}$$

The so-called convergence parameter, μ_0, is a parameter chosen to ensure convergence and stability. The squared error, $e^2(m)$, in least-mean-squares-based algorithms, is desired to be quadratic in W [11: 19-21]. In the acceleration control application, $e(m)$ is equal, therefore, to the acceleration. However, in the intensity control case, the intensity is quadratic in terms of W. This is because F, v, M, and Ω are each linear in W. Therefore, the force term, Fv, and the moment term, $M\Omega$, and, subsequently, the intensity are each quadratic in W. In order to have $e^2(m)$ quadratic in W, $e(m)$ is set equal to the square root of intensity. If Π represents the instantaneous intensity, then the update equation can be expressed as

$$W(m+1)=W(m)-\mu_0\nabla_W\Pi. \tag{4.18}$$

The explicit forms of the gradients are different for each of the various control approaches used in this thesis. Therefore, the developments of the gradients follow in the appropriate sections.

In all control approaches used, it is necessary to determine an appropriate value for the convergence parameter, μ_0. Sommerfeldt [21: 84-89] has shown that, for the filtered-x algorithm, a bound on μ_0--necessary for convergence--is that

$$0<2\mu_0<\frac{2}{\lambda_{max}}, \tag{4.19}$$

where λ_{max} is the largest eigenvalue of the auto-correlation matrix, $E\{\boldsymbol{R}(m)\boldsymbol{R}^T(m)\}$, where $\boldsymbol{R}(m)$ is the input signal, $X(m)$, filtered by the composite transfer function filter, $\boldsymbol{H}(m)$. If the system has 1 error sensor and N control actuators, the control filters have I taps, and the transfer function filters have K taps, then an approximation for this expression can be obtained using the result

$$\lambda_{max}\leq h_{max}^2[N*I*K^2]R_{xx}(0), \tag{4.20}$$

where $R_{xx}(0)$ is the average power of the input signal, and h_{max} is the maximum value of the control path transfer functions' coefficients. Thus a conservative range for μ_0 can be given by

$$0<2\mu_0<\frac{2}{h_{max}^2[N*I*K^2]R_{xx}(0)}. \tag{4.21}$$

Adaptive implementation of this can be facilitated by calculating a value of the average input power, by monitoring the transfer function coefficients, and by, subsequently, updating the value of μ_0 at each time step.

4.2.1 Control of Acceleration

When controlling acceleration, the filtered-x algorithm can be applied in a straightforward manner. The error signal is the acceleration one seeks to control. This acceleration is chosen to be that at position 3 in Figure 3.1, a_3. In this thesis,

one control actuator is used to control the acceleration. There is, therefore, a single control filter and a single control path transfer function filter. Due to the single actuator, the subscript n is dropped. The error signal, $e(m)$, can be represented by

$$e(m)=d(m)+H^T(m)Y(m). \tag{4.22}$$

In summation notation this is expressed as

$$e(m)=d(m)+\sum_{k=0}^{K-1} h_k(m)y(m-k). \tag{4.23}$$

Using the FIR control filter definition this becomes

$$e(m)=d(m)+\sum_{k=0}^{K-1} h_k(m)\sum_{i=0}^{I-1} w_i(m)x(m-k-i). \tag{4.24}$$

The standard development utilizes the assumption that $w_i(m)$ is time invariant, which allows the order of the summations to be interchanged. If this interchange is made, the error signal can be expressed as

$$e(m)=d(m)+\sum_{i=0}^{I-1} w_i\sum_{k=0}^{K-1} h_k(m)x(m-i-k). \tag{4.25}$$

If $r(m)$ is defined to be

$$r(m)=\sum_{k=0}^{K-1} h_k(m)x(m-k), \tag{4.26}$$

then the error signal can be expressed as

$$e(m)=d(m)+\sum_{i=0}^{I-1} w_i\ r(m-i). \tag{4.27}$$

It can be seen that the signal $r(m)$ corresponds to the input signal, $x(m)$, being filtered by the transfer function H, which leads to the name filtered-x. Furthermore, if the vector $\boldsymbol{R}(m)$ is defined as

$$\boldsymbol{R}^T(m)=\left[r(m)\ r(m-1)\cdots r(m-I+1)\right], \tag{4.28}$$

then the error signal can be rewritten in vector notation as

$$e(m)=d(m)+\boldsymbol{W}^T\boldsymbol{R}. \tag{4.29}$$

From this expression the square of the error is found to be

$$e^2(m)=d^2(m)+2d(m)\boldsymbol{R}^T(m)\boldsymbol{W}(m)+\boldsymbol{W}^T(m)\boldsymbol{R}(m)\boldsymbol{R}^T(m)\boldsymbol{W}(m). \tag{4.30}$$

The gradient of this result can be expressed as

$$\nabla_{\boldsymbol{W}} e^2=2\boldsymbol{R}(m)d(m)+2\boldsymbol{R}(m)\boldsymbol{R}^T(m)\boldsymbol{W}(m) \tag{4.31}$$

or

$$\nabla_{\boldsymbol{W}} e^2=2\boldsymbol{R}(m)\left[d(m)+\boldsymbol{R}^T(m)\boldsymbol{W}(m)\right]=2\boldsymbol{R}(m)e(m). \tag{4.32}$$

From this result, the update equation for the control filter coefficients can be expressed as

$$\boldsymbol{W}(m+1)=\boldsymbol{W}(m)-\mu e(m)\boldsymbol{R}(m), \tag{4.33}$$

where

$$\mu = 2\mu_0$$

is a parameter chosen to ensure convergence and stability, and $e(m)$ is the measured acceleration signal. One should note that the error signal used for system identification, $\varepsilon(m)$, is also this acceleration; that is,

$$\varepsilon(m)=e(m)=a_3(m). \tag{4.34}$$

This is because the filtered quantity that the system identification algorithm is trying to model, $\boldsymbol{R}$, corresponds to this acceleration.

4.2.2 Control of Intensity

The intensity control application of the filtered-x algorithm is not as straightforward as the acceleration control. This is because the total, instantaneous intensity is a quadratic quantity in $\boldsymbol{W}$. Thus, to take the gradient of the squared intensity would not be a valid application of the theory. Instead, the gradient with respect to the control filter coefficients is taken of the intensity:

$$\boldsymbol{W}(m+1)=\boldsymbol{W}(m)-\mu_0\nabla_{\boldsymbol{W}}\Pi \tag{4.35}$$

or

$$\boldsymbol{W}(m+1)=\boldsymbol{W}(m)-\mu_0\frac{\partial\Pi}{\partial\boldsymbol{W}}. \tag{4.36}$$

To obtain an expression for the gradient, the intensity can be represented by

$$\Pi = F\nu + M\Omega. \tag{4.37}$$

One should note that

$$F = EI\frac{\partial^3 \xi}{\partial x^3} \qquad \text{and} \qquad M = -EI\frac{\partial^2 \xi}{\partial x^2}, \tag{4.38}$$

where ξ is the transverse displacement. This allows the intensity to be expressed as

$$\Pi = EI\left[\frac{\partial^3}{\partial x^3}\int \nu dt * \nu\right] - EI\left[\frac{\partial}{\partial x}\int \Omega dt * \Omega\right]. \tag{4.39}$$

Use has also been made of the fact that

$$\Omega = \frac{\partial \nu}{\partial x}. \tag{4.40}$$

Further, if ν and Ω are separated into a desired component (the response with no control) and a component due to the control, they can be represented by

$$\begin{aligned} \nu &= \nu_0 + \boldsymbol{H}_\nu^T \boldsymbol{Y} \\ \Omega &= \Omega_0 + \boldsymbol{H}_\Omega^T \boldsymbol{Y}. \end{aligned} \tag{4.41}$$

By interchanging the order of summation, as described in Section 4.2.1, ν and Ω can also be expressed as

$$\begin{aligned} \nu &= \nu_0 + \boldsymbol{W}^T \boldsymbol{R}_\nu \\ \Omega &= \Omega_0 + \boldsymbol{W}^T \boldsymbol{R}_\Omega. \end{aligned} \tag{4.42}$$

Substituting these expressions into Eq. (4.39), the intensity can be expressed as

$$\Pi = EI\left[\frac{\partial^3}{\partial x^3}\int[v_0 + W^T R_v]dt * [v_0 + W^T R_v]\right] - EI\left[\frac{\partial}{\partial x}\int[\Omega_0 + W^T R_\Omega]dt * [\Omega_0 + W^T R_\Omega]\right]. \tag{4.43}$$

Taking the gradient with respect to W of this yields:

$$\nabla_W \Pi = EI\left[\frac{\partial^3}{\partial x^3}\int R_v dt * [v_0 + W^T R_v]\right] + EI\left[\frac{\partial^3}{\partial x^3}\int[v_0 + W^T R_v]dt * R_v\right] - EI\left[\frac{\partial}{\partial x}\int R_\Omega dt * [\Omega_0 + W^T R_\Omega]\right] - EI\left[\frac{\partial}{\partial x}\int[\Omega_0 + W^T R_\Omega]dt * R_\Omega\right]. \tag{4.44}$$

This equation can be simplified by using the expressions for the force and moment. Thus, the gradient can be written as

$$\nabla_W \Pi = EI\frac{\partial^3}{\partial x^3}\int R_v dt * v + F * R_v - EI\frac{\partial}{\partial x}\int R_\Omega dt * \Omega + M * R_\Omega. \tag{4.45}$$

This expression is exact, but it is impractical for implementation on a real-time DSP board. To achieve a practical control scheme for implementation, two sets of heuristic assumptions are used to obtain approximations of this gradient. For the first approximation, the assumptions are made that the third partial derivative with respect to x yields a factor of jk^3, that the first partial derivative with respect to x yields a factor of $-jk$, and that the integral with respect to time yields a factor of $1/j\omega_0$. (j is again $\sqrt{-1}$, k is again the flexural wavenumber, and ω_0 is the driving frequency.) It should be noted that using these assumptions corresponds to assuming time-harmonic excitation and that implementing the resulting algorithm requires a knowledge of the

driving frequency. Using these assumptions in equation (4.45) allows the gradient to be approximated by

$$\nabla_w \Pi \approx \frac{EIk^3}{\omega_0} R_v * v + F * R_v + \frac{EIk}{\omega_0} \Omega * R_\Omega + M * R_\Omega. \tag{4.46}$$

One of the possible limitations is that the signs of the various terms depend on the type of wave which is considered. The signs chosen here correspond to a propagating wave in the $+x$ direction. Obviously, if another type of wave dominates the vibration field, some of the phases in the gradient will be wrong, and that may affect the performance of the control system. Because R_Ω and R_v correspond to an angular velocity and a transverse velocity, respectively, they are related according to:

$$R_\Omega \approx \frac{\partial}{\partial x}\{R_v\}. \tag{4.47}$$

If the derivative is again replaced by $-jk$, R_Ω can be approximated as

$$R_\Omega \approx -jkR_v. \tag{4.48}$$

These results allow the gradient to be approximated as

$$\nabla_w \Pi \approx R_v \left[\frac{EIk^3}{\omega_0} * v + F - j\frac{EIk^2}{\omega_0} * \Omega - jkM \right]. \tag{4.49}$$

This expression cannot be implemented using the real values obtained from accelerometers. If the various signals are assumed to be in phase--an arguable assumption at best, and if the $-jk$ is replaced by k, then the gradient can be approximated by

$$\nabla_W \Pi = R_v \left[\frac{EIk^3}{\omega_0} * v + F + \frac{EIk^2}{\omega_0} * \Omega + kM \right]. \tag{4.50}$$

If this expression is used in the filtered-x algorithm, the update equation can be expressed as

$$W(m+1) = W(m) - \mu e(m) R_v, \tag{4.51}$$

where

$$e(m) = \frac{EIk^3}{\omega_0} * v + F + \frac{EIk^2}{\omega_0} * \Omega + kM \tag{4.52}$$

is the effective error signal for the control algorithm. It should be noted that this is not the effective error signal for the system identification algorithm. In this case the error signal for the system identification algorithm is the velocity term, v. This is because the filtered quantity that this algorithm is trying to model is R_v, the filtered quantity correlating the control output to the velocity. So for this representation of the gradient the error signal used in the system identification is expressed as

$$e(m) = v. \tag{4.53}$$

A simplification of Eq. (4.49) can be obtained by again assuming a time-harmonic, propagating wave in the $+x$ direction. In this case,

$$F = EI \frac{\partial^3 \xi}{\partial x^3} = \frac{EIk^3}{\omega_0} v \qquad \text{and} \qquad M = -EI \frac{\partial^2 \xi}{\partial x^2} = \frac{EIk}{\omega_0} \Omega. \tag{4.54}$$

Using these results in Eq. (4.49) allows the gradient to be approximated by

$$\nabla_W \Pi = \frac{2EIk^2}{\omega_0} R_v [kv + \Omega]. \tag{4.55}$$

The update expression can, therefore, be expressed as

$$W(m+1) = W(m) - \mu e(m) R_v, \tag{4.56}$$

where

$$e(m) = kv + \Omega \tag{4.57}$$

is the effective error signal for the control algorithm. Again, it should be noted that this is not the effective error signal for the system identification algorithm. The system identification error signal is the velocity; that is,

$$e(m) = v. \tag{4.58}$$

This is because the algorithm is trying to model the filtered quantity, R_v.

The terms used in the calculation of the two intensity error functions, Eqs. (4.52) and (4.57), are the same terms used in the calculation of the intensity. For example, the velocity term, v, used in determining both error function signals is calculated as in Eq. (3.10), described in Sections 3.1 and 3.2. It should be noted that the intensity signal is not directly used in the implementation of these control algorithms, but this signal is calculated as a basis of evaluating the effectiveness of the control.

In addition to several possible error signals, three different actuator configurations are considered. These consist of controlling the beam with a control

force, a control moment, or both a force and a moment. Because there are two components to intensity--force and moment--the force-moment configuration for control is believed to be the most promising. The implementation of each of these three strategies is discussed briefly.

4.2.2.1 Control of Intensity with a Force Output

The force output is calculated with one control filter. There is, therefore, a single control filter and a single control path transfer function filter. The force output is sent to two control shakers. This is done in such a way that, if the output to control shaker 1 is represented by y_{c1}, the output to control shaker 2 is represented by y_{c2}, and the force output is represented by y_1, then y_{c1} and y_{c2} are expressed as

$$\begin{aligned} y_{c1}(m) &= y_1(m) \\ y_{c2}(m) &= y_1(m). \end{aligned} \tag{4.59}$$

It is assumed that the control shakers are positioned close to each other--relative to a wavelength--so that the effect on the beam approximates a force applied at a point halfway between the shakers. Although there are two shakers, there is considered to be only one control actuator; this is done to make the development analogous to that of the moment control.

4.2.2.2 Control of Intensity with a Moment Output

The moment output is calculated with one control filter. There is, therefore, a single control filter and a single control path transfer function filter. The moment

output is sent to one control shaker, and the negative of the moment output is sent to the other control shaker. That is, if the output to control shaker 1 is represented by y_{c1}, the output to control shaker 2 is represented by y_{c2}, and the moment output is represented by y_1, then y_{c1} and y_{c2} are expressed as

$$\begin{aligned} y_{c1}(m) &= y_1(m) \\ y_{c2}(m) &= -y_1(m). \end{aligned} \tag{4.60}$$

It is assumed that the control shakers are positioned close to each other--relative to a wavelength--so that the effect on the beam approximates a moment, or couple, applied at a point halfway between the shakers. Again, although there are two shakers, there is only one control actuator.

4.2.2.3 Control of Intensity with Force and Moment Output

The force-moment actuator configuration for control is a superposition of the force configuration and the moment configuration. The force output is calculated with one control filter, and the moment output is calculated with another control filter. There are, therefore, two control filters and two control path transfer function filters. The force output is sent to both shakers. The moment output is sent to one shaker and the negative of the moment output is sent to the other shaker. That is, if the output to control shaker 1 is represented by y_{c1}, the output to control shaker 2 is represented by y_{c2}, the force output is represented by y_1, and the moment output is represented by y_2, then y_{c1} and y_{c2} are expressed as

$$y_{c1}(m)=y_1(m)+y_2(m)$$
$$y_{c2}(m)=y_1(m)-y_2(m). \tag{4.61}$$

4.2.3 Summary of Control Update Equations

The update equations to be used in this thesis are common to all strategies for control. The system identification filter update equation is expressed as

$$\hat{\Theta}(m+1)=\hat{\Theta}(m)+\frac{a\Phi(m)}{b+\Phi^T(m)\Phi(m)}\left[e(m)-\hat{\Theta}^T(m)\Phi(m)\right], \tag{4.62}$$

and the control filter update equation is expressed as

$$W(m+1)=W(m)-\mu e(m)R(m). \tag{4.63}$$

The variations in control strategies result from the definition of the error signals and from the number of control filters employed in the strategy.

In the acceleration control strategy, the error signals are defined as

$$e(m)=e(m)=a_3(m), \tag{4.64}$$

and the vectors in the update equations are defined as

$$\hat{\Theta}^T(m)=\left[h_{10}(m)\cdots h_{1(k-1)}(m)\, h_{20}(m)\cdots h_{2(K-1)}(m)\right], \tag{4.65}$$

$$\Phi^T(m)=\left[y(m)\cdots y(m-K+1)\, x(m)\cdots x(m-K+1)\right], \tag{4.66}$$

$$W^T(m)=\left[w_1(m)\cdots w_{(l-1)}(m)\right], \tag{4.67}$$

and

$$R^T(m) = [r(m) \cdots r(m-I+1)]. \tag{4.68}$$

In the various intensity strategies, the control update error signals are expressed as

$$e(m) = \frac{EIk^3}{\omega_0} * v + F + \frac{EIk^2}{\omega_0} * \Omega + kM \tag{4.69}$$

or

$$e(m) = kv + \Omega, \tag{4.70}$$

and the system identification update error signal for both instances is expressed as

$$e(m) = v. \tag{4.71}$$

For the force actuator configuration and for the moment actuator configuration, the update equation vectors have the same form, and they are expressed as

$$\hat{\Theta}^T(m) = [h_{10}(m) \cdots h_{1(K-1)}(m)\, h_{20}(m) \cdots h_{2(K-1)}(m)], \tag{4.72}$$

$$\Phi^T(m) = [y(m) \cdots y(m-K+1)\, x(m) \cdots x(m-K+1)], \tag{4.73}$$

$$W^T(m) = [w_1(m) \cdots w_{(I-1)}(m)], \tag{4.74}$$

and

$$R^T(m) = [r(m) \cdots r(m-I+1)]. \tag{4.75}$$

For the force-moment actuator configuration, the update equation vectors are expressed as

$$\hat{\Theta}^T(m) = \left[h_{10}(m) \cdots h_{1(K-1)}(m)\, h_{20}(m) \cdots h_{2(K-1)}(m)\, h_{30}(m) \cdots h_{3(K-1)}(m) \right], \tag{4.76}$$

$$\Phi^T(m) = \left[y_1(m) \cdots y_1(m-K+1)\, y_2(m) \cdots y_2(m-K+1)\, x(m) \cdots x(m-K+1) \right], \tag{4.77}$$

$$W^T(m) = \left[w_{10}(m) \cdots w_{1(I-1)}(m)\, w_{20}(m) \cdots w_{2(I-1)}(m) \right], \tag{4.78}$$

and

$$R^T(m) = \left[r_1(m) \cdots r_1(m-I+1)\, r_2(m) \cdots r_2(m-I+1) \right]. \tag{4.79}$$

Chapter 5

EXPERIMENTAL METHOD

The experimental method is described in this chapter. The chapter is divided into two parts: Section 5.1 discusses the experimental setup and Section 5.2 discusses the experimental procedure.

5.1 The System

The system is divided into two parts: the system being controlled and the controlling system. Section 5.1.1 describes the structural system being controlled, including the beam, the terminations, and the support system. Section 5.1.2 describes the control system hardware.

5.1.1 Beam Description

The structure to be controlled in this study consists of a thin-walled, square, hollow steel beam; one end of which is embedded in a box of sand. The other end is supported with a compliant rubber band, which is fastened to an overhead support structure. This rubber band is used to support the static load, and it is assumed that the rubber band does not significantly alter the dynamic loading on the beam.

The steel beam has been found to have the following geometrical and mechanical properties: density (ρ) = 7.70×10^3 kg/m^3; cross sectional area (A) =

74.0×10^{-6} m^2; modulus of elasticity (E) = 187×10^9 Pa; and moment of inertia of the cross section (I) = 2.71×10^{-9} m^4.

One end of the beam is embedded in a box of sand in order to introduce absorption at the boundary and, hence, reduce the magnitude of the reflection coefficient from the value of 1.0 associated with a purely free termination. A lossless beam and a reflection coefficient of 1.0 at the boundary results in a standing wave field only and, therefore, only reactive (or imaginary) intensity is generated. Reducing the reflection coefficient at the boundary reduces the reflected wave and, therefore, allows the propagating wave component to dominate the wave field. This results in an active (or real) intensity component. If the termination is anechoic, corresponding to the reflection coefficient having a value of 0.0, then the intensity is entirely active. Previous studies on beams with the same properties and similar terminations have shown that the reflection coefficient is approximately 0.254+j0.044 at 5000 Hz and 0.536+j0.058 at 500 Hz [17,23]. Therefore, for the frequency range used for this study (140 Hz to 520 Hz), a combination of active and reactive intensity is expected.

The beam is excited at its free end with a Ling Dynamic Systems (LDS) model V203 magnetic driven vibrator. A sinusoidal signal is generated by a Wavetech model 75 arbitrary waveform generator. This signal is passed through a BGW Systems model 200 professional power amplifier. The signal is then sent to the LDS V203 shaker, which excites the beam with a sinusoidal vibration.

The LDS V203 shaker is connected to the beam by a stinger to insure the delivery of a moment-free transverse force to the beam. The stinger is relatively

flexible in its transverse direction, in order to minimize the transfer of any moment to the beam due to misalignment. This stinger is constructed with a short piece of 20-gage steel wire soldered into holes drilled in two bolts. The bolts are the same size as the tapped mounting hole in the shaker. One bolt is threaded into the mounting hole in the shaker, and the other bolt is glued with epoxy to the beam.

5.1.2 Control System

The control system consists of three parts: the input sensors, the processor, and the output actuators. A schematic diagram of the control system is found in Figure 5.1. This figure shows the various parts of the control system and the connection paths. Section 5.1.2.1 discusses the input sensor hardware; Section 5.1.2.2 discusses the processor hardware; and Section 5.1.2.3 discusses the output actuator hardware.

5.1.2.1 The Inputs

The six input signals to the control system originate from 5 accelerometers and the signal from the signal generator which drives the excitation shaker. The signals from the accelerometers are used to calculate the error signals (the error signal in acceleration control is the third acceleration signal). The signal from the signal generator is used as the control filter input, $x(m)$.

The five accelerometers used to calculate the error signals are PCB Piezotronics, Inc. (PCB) model 336A accelerometers. The serial numbers of the

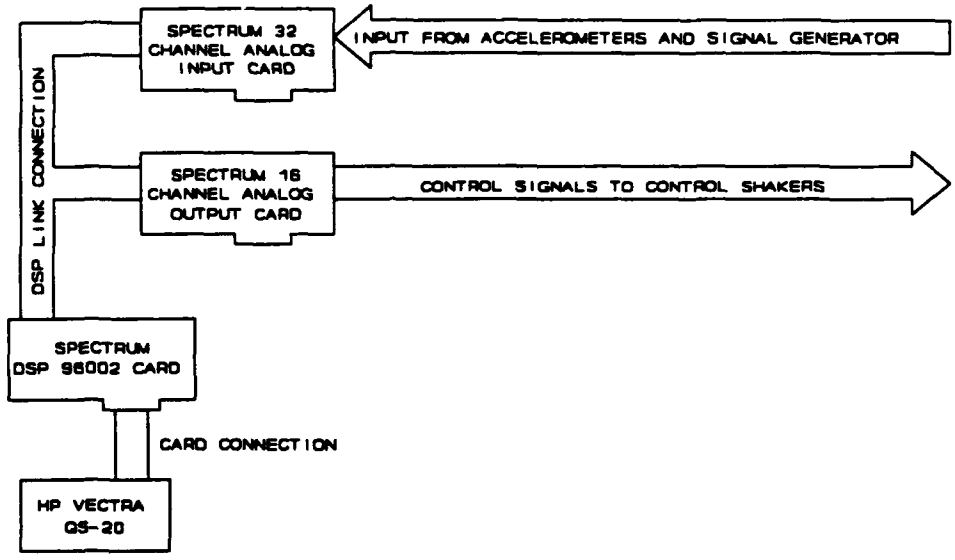

Figure 5.1 Schematic Diagram of Control System.

accelerometers, in order of position from the free end, are #1136, #1156, #1140, #1141, and #1142. The response calibration of each accelerometer, as described in section 3.3, is performed relative to accelerometer #1136. The complete table of calibration constants calculated is given in the Appendix. The accelerometer signals pass through a conditioning amplifier, which is a PCB 483BO7 12-channel amplifier. This amplifier is chosen for compatibility with the PCB accelerometers. The control filter input signal is also passed through the conditioning amplifier.

After being amplified, the six input signals are sent to a Spectrum Signal Processing Inc. 32 channel analog input board. This board consists of a 12 bit A/D converter, and it allows a 4 channel sample and hold operation [24]. The input

board has a dynamic range of ± 2.5 V. It is designed to interface with Spectrum's line of Digital Signal Processing (DSP) boards.

5.1.2.2 The Processor

The processing loop includes the input board, the DSP board, the host computer, and the output board. The input board is the Spectrum 32 channel analog input board described previously. The DSP board is a Spectrum Signal Processing Inc. DSP 96002 board, which is built around a Motorola XSP96002RC33 chip. The processor is a 96-bit floating point processor. The DSP 96002 communicates with the input and output boards over a 16 bit data bus. The output board is a Spectrum Signal Processing Inc. 16 Channel analog output card.

The Spectrum boards--input, output, and DSP--all require a host PC. The host PC used is a Hewlett Packard Vectra QS/20, 386-based machine. The host PC provides power for the boards, as well as a platform for generating the code to be downloaded to the DSP board. The DSP board data and memory registers are also monitored via the host PC.

5.1.2.3 The Outputs

The outputs consist of the necessary control output signals. For the case of acceleration control there is only one such output signal. For the case of intensity control (force only, moment only, or force and moment) there are two such output signals.

These output signal(s) are sent through a Spectrum Signal Processing Inc. 16 channel analog output card. The output board is a 12-bit D/A converter and allows 16 channels of simultaneous output through the use of a double buffer output system. If the double buffer is used, the signals are sent to a buffer and at the proper time all of the signals are released simultaneously. The output board has a dynamic range of approximately ± 8.19 V [25].

The output signal(s) are amplified by means of a BGW Systems model 200 professional power amplifier.

After amplification, the signal(s) are used to drive the control shaker(s). The control shakers are LDS model V102 magnetic driven vibrators. The V102 shakers employ stingers, whose construction is similar to that of the V203's stinger. The only difference is that the bolt size is different, due to the fact that the tapped hole in the V102 shaker has a different size. Again, the bolt on one end of the stinger is mounted to the shaker, and the bolt on the other end of the stinger is glued with epoxy to the beam.

5.2 The Experimental Procedure

This section describes the experimental procedure. The measurement of the structural intensity is conducted at one frequency, 300 Hz. This frequency is chosen because it is thought that the spacing and timing regarding the finite difference techniques are optimal at 300 Hz. The adaptive vibration control investigation uses frequencies grouped around 300 Hz. The adaptive vibration control study is

conducted at six frequencies, three of which are found to be resonances of the beam system: 140 Hz, 296 Hz, and 488 Hz. Three additional, off-resonance frequencies are also studied: 200 Hz, 340 Hz, and 520 Hz. Section 5.2.1 describes the structural intensity measurements, and Section 5.2.2 describes the adaptive vibration control implementation.

All signal analysis is done using a HP 3566A signal analyzer, which is referred to as the analyzer. The HP 3566A is a frequency analyzer that needs a host pc. The host pc is the HP Vectra QS/20 described previously. This analyzer uses the MS-DOS© operating system and a Microsoft© Windows-based user interface.

5.2.1 Intensity measurement

This section describes the study of the structural intensity measurement. An attempt is made to correlate frequency spectra of the calculated output and input structural intensities, in order to verify the algorithm developed in Chapter 3. The output intensity refers to the total, instantaneous intensity measured at the accelerometer array and calculated using this algorithm. The input intensity is a measure of the intensity input to the beam. It is measured at the excitation shaker. The assumption is made that at the excitation shaker the intensity is dominated by the force term. For this reason, the force term, Fv, of the input intensity is measured, using a force gauge and an accelerometer. The experimental configuration is as shown in Figure 5.2.

The input intensity is calculated by multiplying the force at the input by the velocity at the input. The force at the input is found using a PCB 208B force trans-

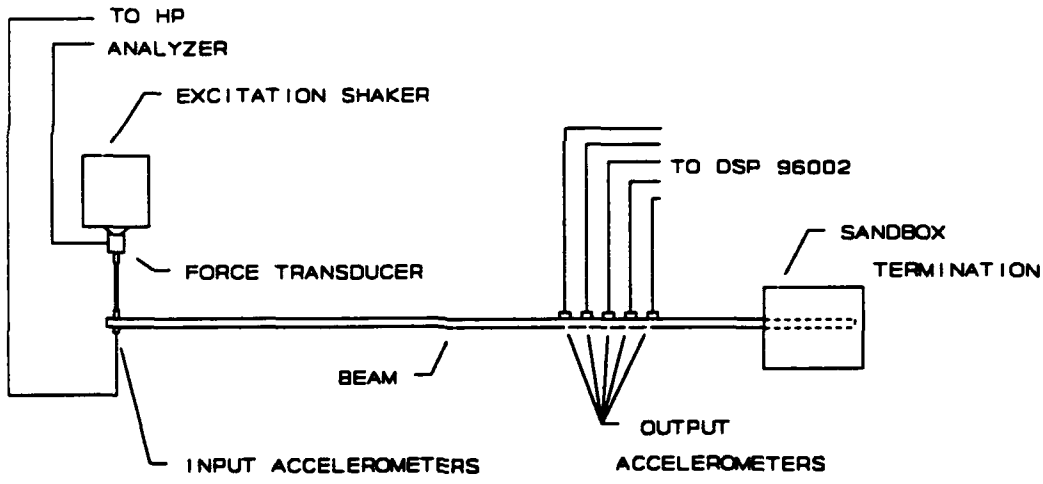

Figure 5.2 Experimental Setup for Intensity Measurement.

ducer, positioned between the shaker and its stinger. This signal is conditioned using the PCB 483BO7 amplifier described previously. The signal is then sent to the analyzer. The velocity at the input is found by integrating an acceleration signal at the input. This integration is performed in the frequency domain, through multiplying by $1/j\omega$. The acceleration signal is found using a PCB 303A13 accelerometer. The acceleration signal is conditioned through the PCB 483BO7 amplifier described previously. This acceleration signal is then sent to the analyzer.

The input intensity ideally would be calculated by first transforming the acceleration into the frequency domain. Integration of this acceleration signal would then be performed in the frequency domain, by means of multiplying by $1/j\omega$. Then, this velocity signal would be transformed to the time domain. This time sequence of the velocity signal would be multiplied by the time sequence of the force in order to obtain a time sequence of the input intensity.

However, the vibration at the output sensor array is assumed to be of one frequency. (Recall the assumption made in Chapter 3 to facilitate double time integration of the acceleration signals.) Because the output intensity is calculated using this single frequency assumption, the input intensity is also calculated using this assumption, to facilitate comparison. Therefore, the input intensity is calculated by transforming both the acceleration and the force signals into the frequency domain. Then both signals are multiplied by $(j\omega)^2$. Both signals are then divided by $(j\omega_0)^2$, so that the result is to multiply both signals at all frequencies by ω^2/ω_0^2. This has the effect of twice differentiating the two signals with a broadband assumption, followed by double integrating the two signals with a single frequency assumption. The acceleration signal is then divided by $j\omega$ in order to integrate to a velocity signal. Then, the force and velocity signals are transformed to the time domain. The two time signals are then multiplied, and this input intensity signal is transformed to the frequency domain, for comparison.

The output intensity is calculated on the DSP 96002 and output via the output board. The output intensity is the total, instantaneous intensity measured at the accelerometer array and calculated as described in Chapter 3. The appropriate DSP 96002 program is run and the intensity signal is input to the analyzer. The analyzer then performs an FFT on the signal in order to allow a frequency domain comparison with the measured input intensity.

The two frequency representations, input and output intensity, are compared for relative magnitude and phase. A discussion of the data obtained from these measurements is presented in Section 6.1.

5.2.2 Control

This section describes the experimental procedure involved in the study of the adaptive control of structural intensity. Section 5.2.2.1 describes the data which is recorded, and Section 5.2.2.2 describes the procedure of data acquisition.

5.2.2.1 Description of Control Data

The study investigates the ability of the algorithms developed to control intensity. The study also investigates the effectiveness of the algorithms relative to the control of acceleration. The gauge of this effectiveness is an acceleration signal close to the termination, referred to as the downstream accelerometer. This method of evaluation is chosen because, as is noted in Section 2.2, controlling intensity should greatly reduce the farfield vibration. The downstream acceleration signal is obtained from a PCB 303A13 accelerometer, and the signal is conditioned using the PCB amplifier described above.

Adaptive vibration control is performed at six different frequencies. Of these six, three are at resonances of the beam structure: 140 Hz, 296 Hz, and 488 Hz. The other three frequencies are off-resonance: 200 Hz, 340 Hz, and 520 Hz.

Values of the flexural wavelength of vibration in the beam, λ, of the flexural wavenumber, k, of $\lambda/4$, and of $\lambda/2$ are given for each of these six frequencies in Table 5.1. If an error sensor is at a distance from the control actuator less than $\lambda/4$, then it is assumed to be in the nearfield of the control actuator. At these distances, the sensor will measure the exponentially decaying waves associated with the nearfield. If, however, the error sensor is at a distance of $\lambda/2$ or greater from the control actuator, then it is assumed to be in the farfield of the actuator. The error sensor is not in the field dominated by the exponentially decaying waves. For the beam in this study, it is possible to position the error sensor in the nearfield or the farfield of the control actuator, but positioning the error sensor in the farfield of the actuator places it in the nearfield of the sandbox termination. To avoid the confusion

Table 5.1 Flexural Wavelength, Flexural Wavenumber, $\lambda/4$, and $\lambda/2$ of Beam Structure at Frequencies of Interest.

Freq. Hz	λ cm	k m^{-1}	$\lambda/4$ cm	$\lambda/2$ cm
140	116.	5.43	29.0	58.0
200	96.9	6.49	24.2	48.5
296	79.6	7.90	19.9	39.8
340	74.3	8.46	18.6	37.2
488	62.0	10.1	15.5	31.0
520	60.1	10.5	15.0	30.1

that this presents, in this thesis distances from the control actuator of $\lambda/2$ and greater are referred to as relatively far from the control actuator. Likewise, positions in the nearfield of the control actuators are referred to as relatively near to the control actuators.

In an attempt to gain a better understanding of the phenomena occurring, the position of the control actuator, relative to the excitation shaker is varied. The two positions of the control actuators are referred to as near to and far from the excitation shaker. This convention is used without consideration of the nearfield or farfield of the excitation shaker.

There are four hardware setups investigated. These are diagrammed in Figure 5.3, where X is the distance from the excitation shaker to the center error accelerometer and Y is the distance from the excitation shaker to the intensity control actuator. The distance from the intensity control actuator to the center error accelerometer is, therefore, X-Y. The first setup is configured with the control shakers far from the excitation shaker (Y=31 cm); it also has the error accelerometer array relatively far from the control shakers (X-Y=60 cm). The second setup has the control shakers positioned far from the excitation shaker (Y=31 cm), but the error accelerometer array is relatively near to the control shakers (X-Y=15 cm). The third setup is configured with the control shakers near to the excitation shaker (Y=16 cm), and it has the error accelerometer array relatively far from the control shakers (X-Y=75 cm). The fourth setup has the control shakers positioned near to the excitation shaker (Y=16 cm), and it has the error accelerometer array relatively near to the

control shakers (X-Y=15 cm). These set-ups are intended to investigate the influence of farfield effects and nearfield effects.

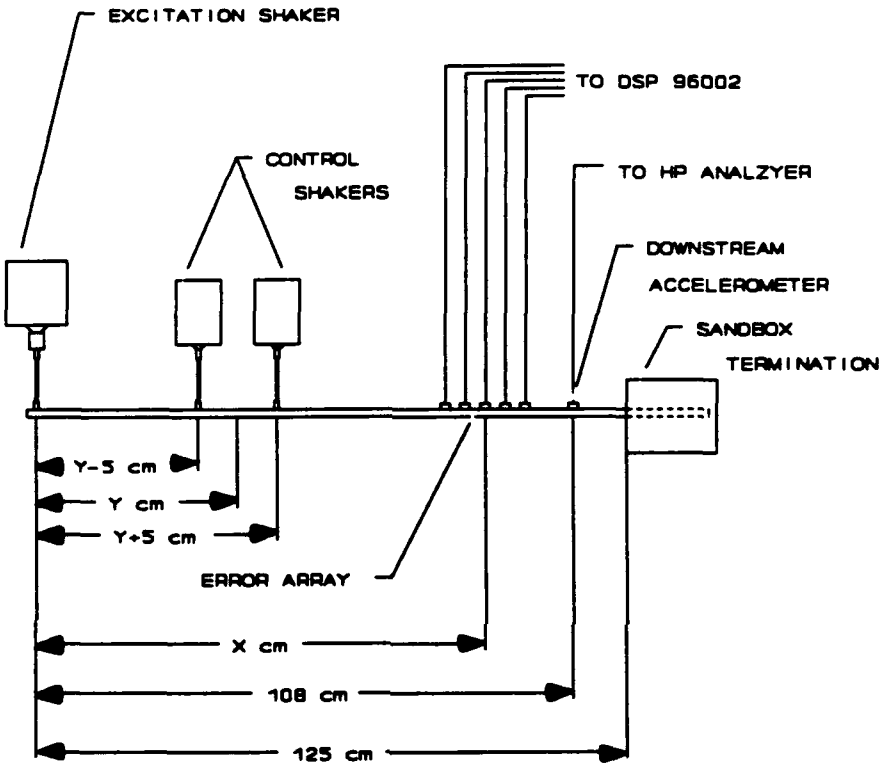

Figure 5.3 Schematic of Four Control Setups.

At each of the twenty-four setup/frequency permutations, seven control strategies are implemented: (1) acceleration control, (2) and (3) intensity control using a force actuator only for each of the two gradients developed in Section 4.2.2, (4) and (5) intensity control using a moment actuator only for each of the two gradients, and (6) and (7) intensity control using both force and moment actuators for each of the two gradients. This amounts to 168 control scenarios.

The data recorded for each control scenario consists of the control error signal (specific to the control scenario), the structural intensity calculated from the accelerations measured from the sensor array, and the downstream acceleration. The same data without control is also taken at each setup/frequency permutation, consisting of the acceleration error signal, each of the two intensity control effective error signals, total intensity, and downstream acceleration.

Upon initial implementation of the various intensity control schemes, it is noticed that the error function signals quite often contain high frequency noise. This noise is seen at harmonic frequencies of the excitation frequency. On certain tests, the harmonic noise is as high or higher than the signal at the excitation frequency. In order to eliminate this high frequency noise, the error function signal is passed through a digital lowpass filter. This digital lowpass filter is designed using a Hamming window as described in Oppenheim and Schafer [26: 444-457]. A different filter is designed for each frequency considered.

5.2.2.2 Description of Control Data Acquisition

This section describes the routine followed when collecting the data described in section 5.2.2.1. All of the data are recorded and analyzed using the HP 3566A analyzer described above. For each data signal recorded, a uniform average of 50 power spectra is recorded.

At each setup/frequency permutation, the PCB conditioning amplifier gains are set to ensure that the ± 2.5 V maximum range of the input board is not exceeded.

The five channels conditioning the error accelerometer array are set to the same gain.

After the conditioning amplifier gains are set, the data are saved without control. Following this, each of the control scenarios is implemented in turn. With a given scenario running, the intensity signal, the appropriate error signal, and the downstream acceleration signal are recorded. A discussion of the results obtained from these measurements is given in Section 6.2.

Chapter 6

DISCUSSION OF EXPERIMENTAL RESULTS

This chapter examines the experimental results obtained in the study. Section 6.1 describes the data obtained in the intensity measurements. Section 6.2 describes the adaptive vibration control achieved through the filtered-x algorithm.

6.1 Discussion of Intensity Measurement

This section discusses the validity of the intensity measurements. The data supporting these measurements are acquired in the manner described in Section 5.2.1.

The relative magnitudes of the two intensity signals are discussed first. The absolute magnitudes are not discussed because the output intensity signal is scaled to utilize the resolution of the output board. The magnitude of the output intensity is shown in Figure 6.1, and the magnitude of the input intensity is shown in Figure 6.2. When one looks at these two traces four things require explanation: the noise levels of the two traces, the general positive slope of the input intensity trace, the existence of a dominant 300 Hz peak on the output intensity trace, and the presence of a large dc peak on the input intensity trace.

The first issue to be discussed is that the noise appears to be higher on the output intensity trace. This is reasonable because of the greater number of transducers involved in this measurement and because of the number of approximations and calculations involved in the finite difference schemes used.

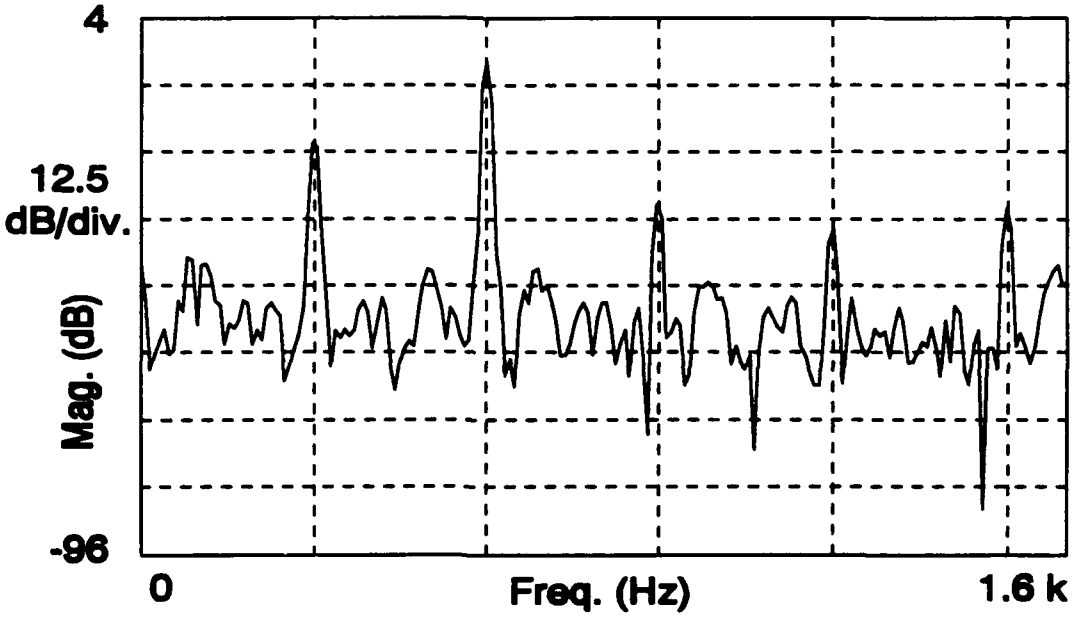

Figure 6.1 Linear Spectrum of Output Intensity at 300 Hz.

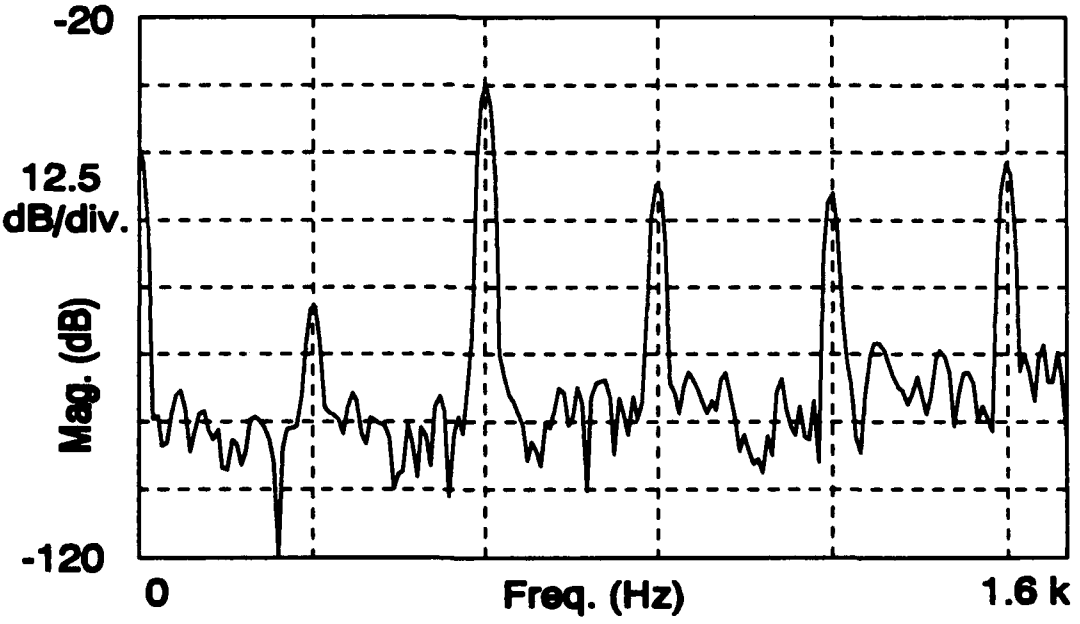

Figure 6.2 Linear Spectrum of Input Intensity at 300 Hz.

The second issue for discussion--the positive slope of the input intensity trace--can be attributed to the method used to determine the measured output intensity. The higher noise level associated with the output intensity covers up any slope in that trace. Also, multiplying the input signals by $(j\omega)^2$ would introduce a slope of 12 dB/octave, which is comparable to the slope appearing in the input intensity trace.

The third issue--the dominant 300 Hz peak on the output intensity trace--is thought to be error introduced through use of the finite difference approximations.

Finally, the fourth issue for discussion--the large dc peak on the input trace--is thought to be due to the large dc bias of the force transducer. With no excitation, the force transducer gives a dc peak approximately 75 dB above the noise level. This is opposed to a representative accelerometer which, with no excitation, gives a dc peak of approximately 45 dB above the noise level. Because the output intensity is measured only with accelerometers the dc bias would not be as great.

The phases, calculated as arctan(Im/Re), of the two signals are also investigated. The phase of the output intensity is shown in Figure 6.3, and the phase of the input intensity is shown in Figure 6.4. When these phases are compared, one can see that, at the three important frequencies (0, 300, and 600 Hz), the phases differ by approximately 180°. This is due to the fact that the positive direction for the input intensity was opposite to that used for the output intensity. Taking this difference in orientation into account, the phase differs by 5° or 6°.

The output intensity is thought to be a valid measure due to this correlation with input intensity. The fact that the phases are almost matched and the general

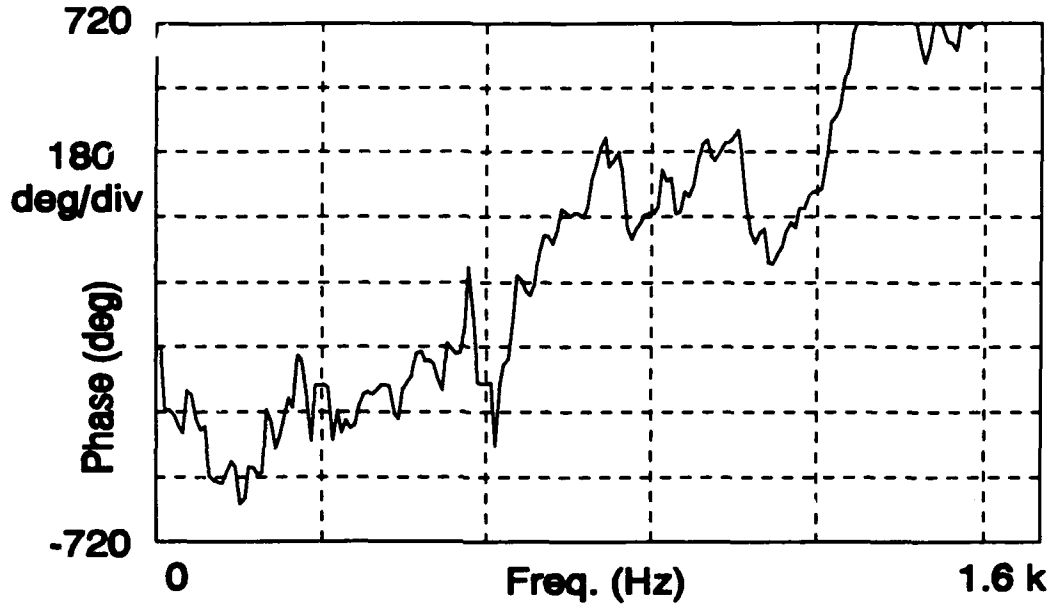

Figure 6.3 Phase of Output Intensity at 300 Hz.

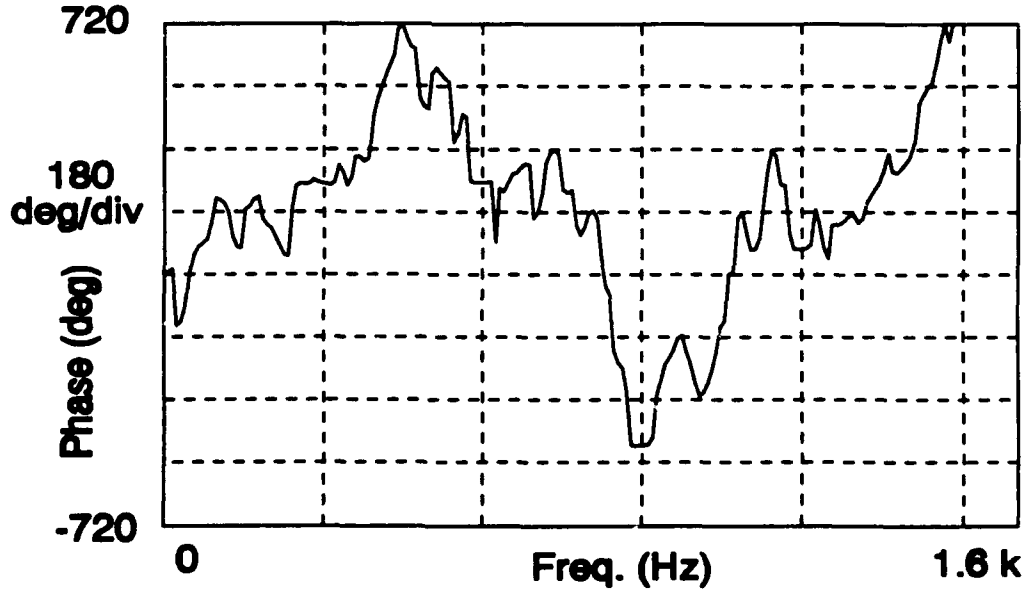

Figure 6.4 Phase of Input Intensity at 300 Hz.

agreement of the magnitude peaks support this claim. There is, however, a great deal of noise introduced into the intensity signal measured by the accelerometer array.

6.2 Discussion of Control Results

The results obtained from the various control scheme measurements are discussed in this section. There are three items which should be noted. The first is that for convenience in examining the following frequency domain plots, the vertical divisions are placed at multiples of the driving frequency. The second is that due to limits of the output board, the intensity and error function signals are scaled to avoid clipping while realizing the resolution potential of the D/A converter. This scaling of the signals is invariant within a given setup/frequency permutation. The result is that specific values are compared within a setup/frequency permutation; however, only relative reductions are to be compared otherwise. The third point to note is that for convenience of discussion, the gradients of intensity that were developed in Section 4.2.2 are referred to as the long error function and the short error function. The error function expressed in Eq. (4.52) is referred to as the long error function:

$$e(m)=\frac{EIk^3}{\omega_0}*v+F+\frac{EIk^2}{\omega_0}*\Omega+kM. \tag{6.1}$$

The error function expressed in Eq. (4.57) is referred to as the short error function:

$$e(m)=kv+\Omega. \tag{6.2}$$

There are seven aspects of the control results which are examined. Section 6.2.1 is a discussion of the acceleration control, which works better with the error sensor positioned relatively far from, rather than relatively near to, the control actuator. Section 6.2.2 discusses the general trends of intensity control with the error sensor positioned relatively far from the control actuator. Section 6.2.3 examines intensity control with the error sensor positioned relatively near to the control actuator. Section 6.2.4 is a discussion of the general trend of frequency dependence of the intensity control. Section 6.2.5 is a discussion of the issues associated with the long error function, while Section 6.2.6 examines the issues associated with the short error function. Finally, Section 6.2.7 discusses the trends in actuator configuration dependence in intensity control. It describes which of the actuator configurations--force actuator only, moment actuator only, or force and moment actuators--yields the best performance.

The various hardware setups that were examined in Section 5.2.2.1 are given in Table 6.1 for quick reference.

6.2.1 Acceleration Control

This section examines the differences between controlling acceleration with the error sensor positioned relatively far from and relatively near to the control actuator. In Section 2.2 it is noted that the control should perform better with the error

Table 6.1 Hardware setups versus positions of error sensor and control actuator.

Hardware Setup #	Error Sensor Relative to Control Actuator	Control Actuator Relative to Excitation Shaker
1	far	far
2	near	far
3	far	near
4	near	near

sensor positioned relatively far from, rather than relatively near to, the control actuator.

If one examines Figures 6.5 and 6.6, it can be seen that the control scheme reduces the error acceleration signal comparably. In each case the error acceleration signal, at the driving frequency, was reduced by over 60 dB. However, if one examines Figures 6.7 and 6.8, this comparable reduction in the error acceleration does not result in comparable reductions in the downstream acceleration signal. In Figure 6.7 it can be seen that controlling acceleration with the error sensor positioned relatively far from the control actuator results in more than a 50 dB drop in the downstream acceleration signal, while in Figure 6.8 it can be seen that controlling acceleration with the error sensor positioned relatively near to the control actuator results in approximately a 20 dB drop in the downstream acceleration signal. These results are in agreement with the expectations discussed in Section 2.2.

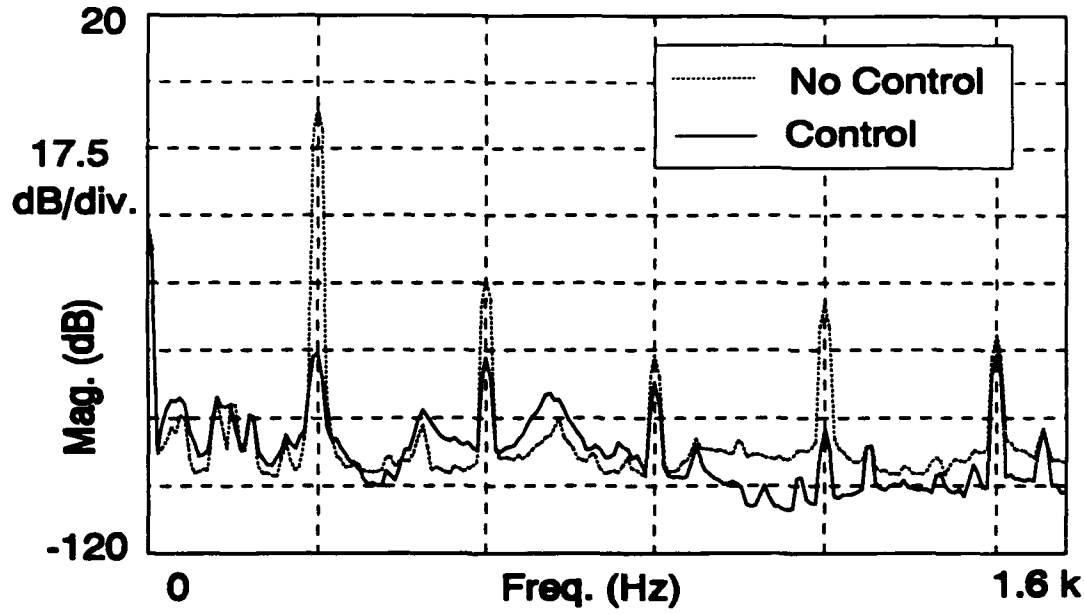

Figure 6.5 Error Acceleration, Acceleration Control, 296 Hz, Setup 3.

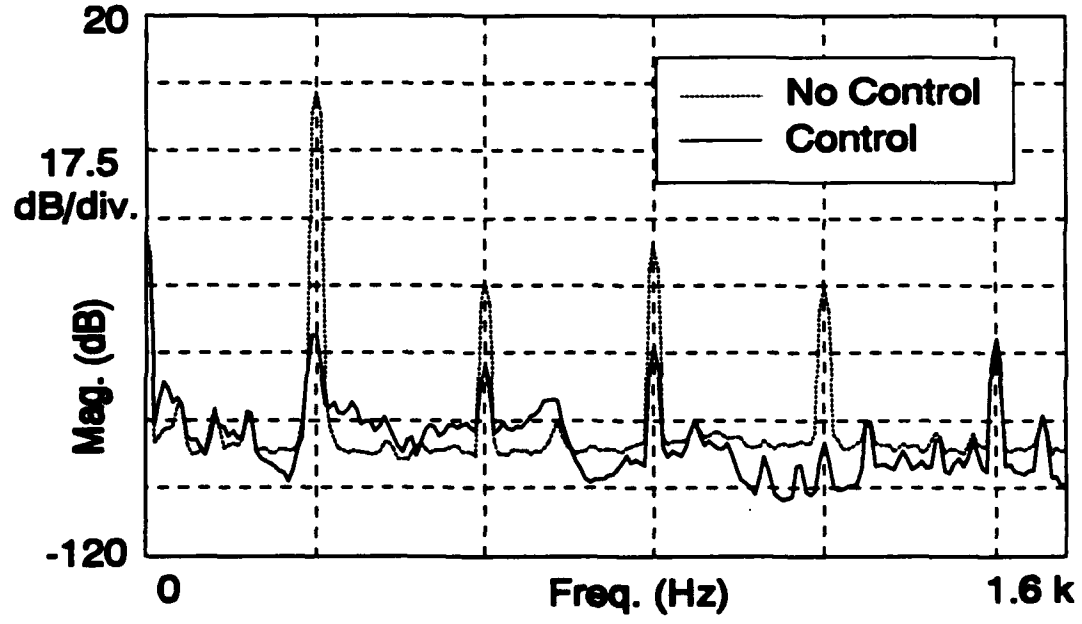

Figure 6.6 Error Acceleration, Acceleration Control, 296 Hz, Setup 4.

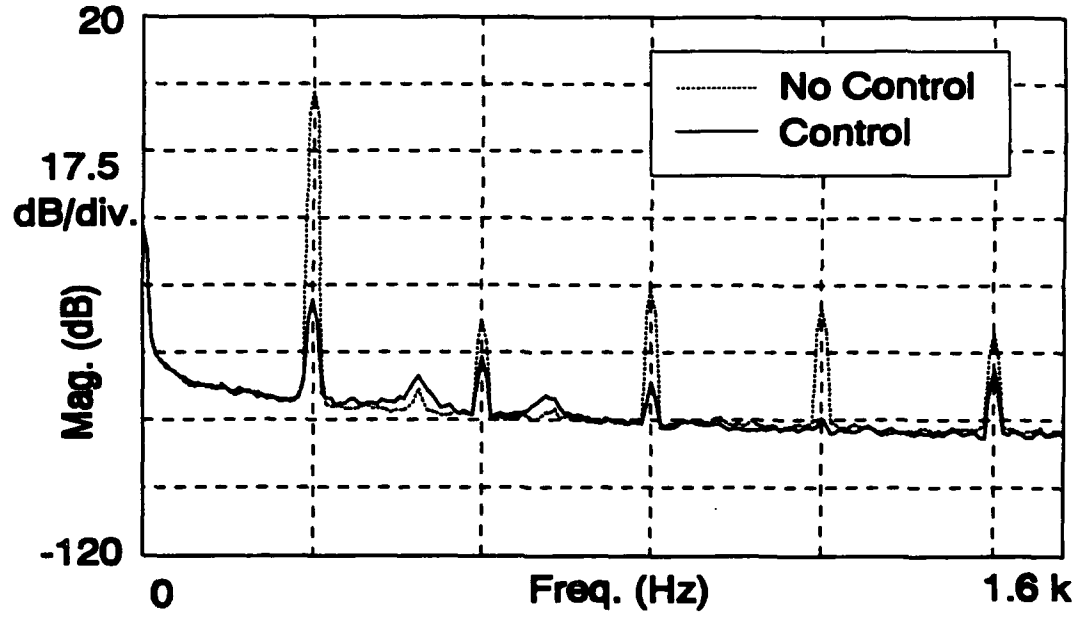

Figure 6.7 Downstream Acceleration, Acceleration Control, 296 Hz, Setup 3.

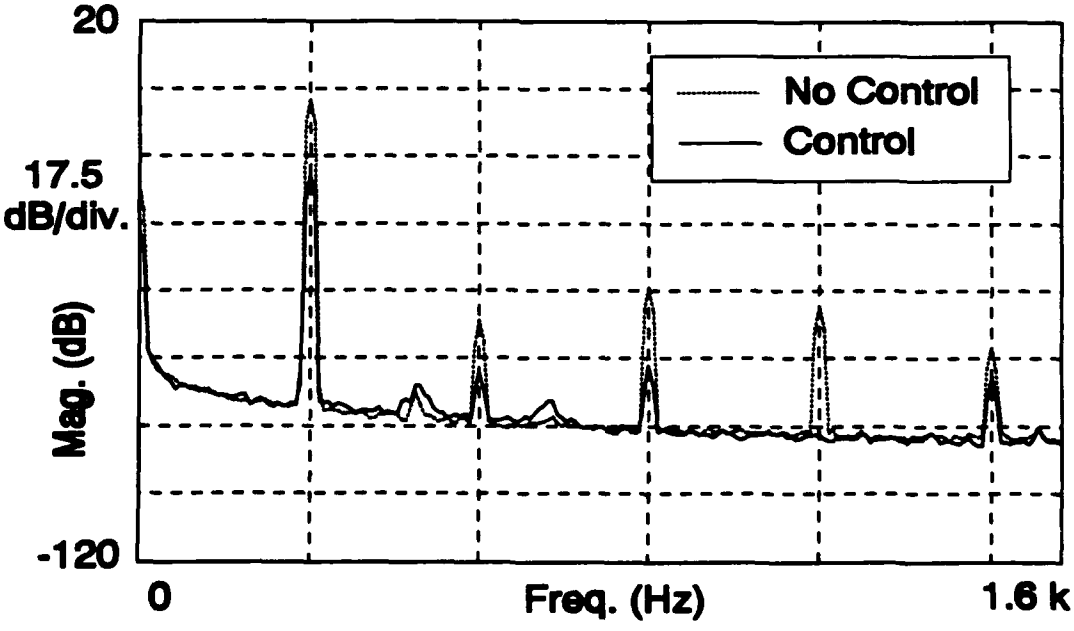

Figure 6.8 Downstream Acceleration, Acceleration Control, 296 Hz, Setup 4.

6.2.2 Intensity Control in the Farfield

This section discusses intensity control with the error sensor positioned relatively far from the control actuators. It is noted in Section 2.2 that the intensity control should perform as well as the acceleration control with the error sensor located in the farfield.

If one examines Figure 6.9, it can be seen that the short error function signal is reduced by approximately 50 dB. One can observe the roll off of the error function signal as a result of the lowpass digital filter implemented as described in Section 5.2.2.1. The intensity signal, as shown in Figure 6.10, is reduced as well. The peak

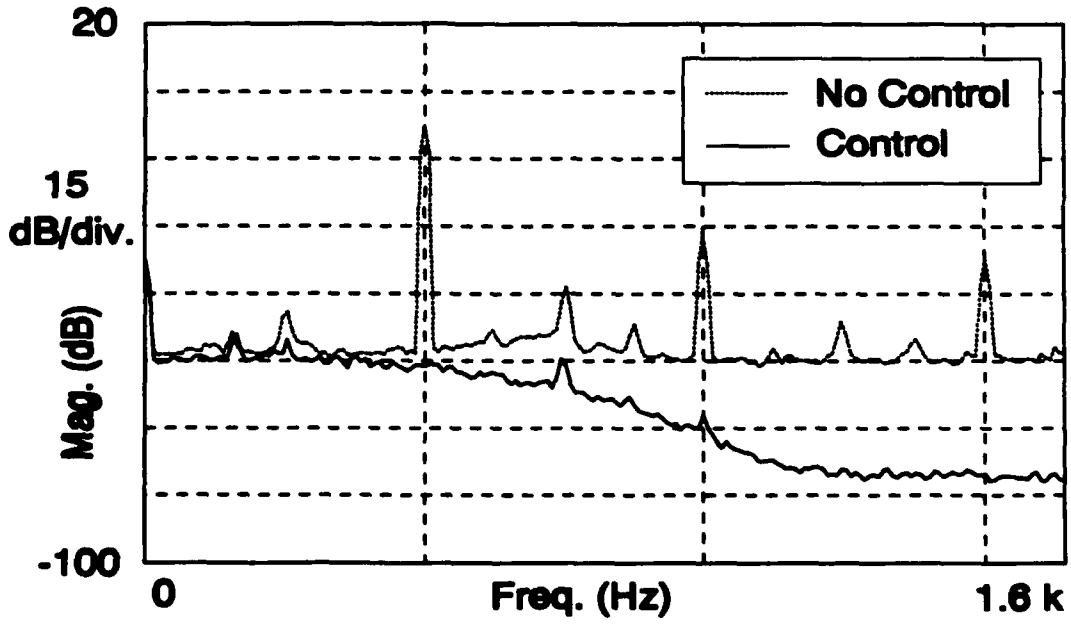

Figure 6.9 Error Function, Short Error Intensity Control, Force and Moment Actuators, 488 Hz, Setup 3.

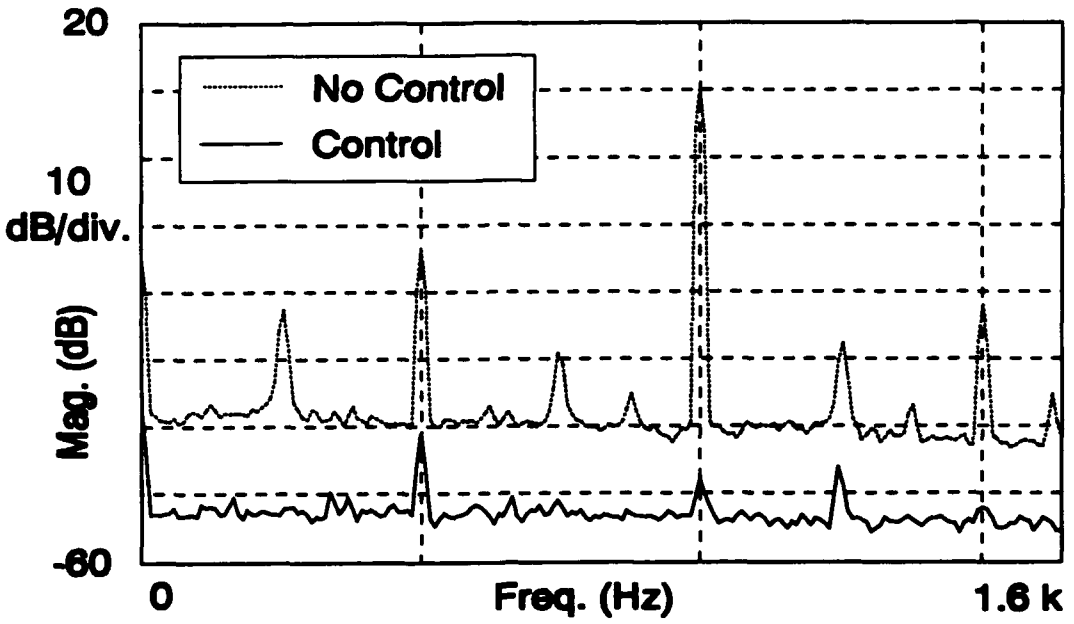

Figure 6.10 Intensity Signal, Short Error Intensity Control, Force and Moment Actuators, 488 Hz, Setup 3.

at $2\omega_0$, 976 Hz, is reduced on the order of 55 dB, while the dc value is reduced approximately 25 dB. The downstream acceleration signal is reduced approximately 20 dB, see Figure 6.11, through implementation of this intensity control scheme. This is in contrast to the more than 40 dB reduction in the downstream acceleration achieved through the implementation of the acceleration control scheme, as shown in Figure 6.12.

The fact that the acceleration control performs better than the intensity control when the error sensor is positioned relatively far from the control actuators is anticipated. This is because of the noise introduced into the error function signal due to the numerical noise associated with the finite difference schemes.

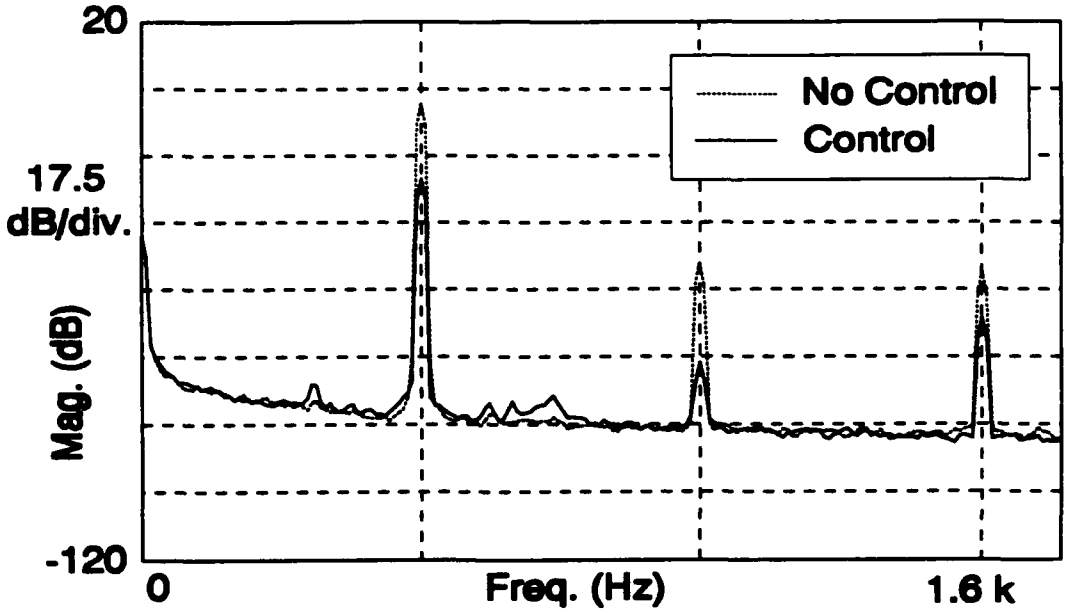

Figure 6.11 Downstream Acceleration, Short Error Intensity Control, Force and Moment Actuators, 488 Hz, Setup 3.

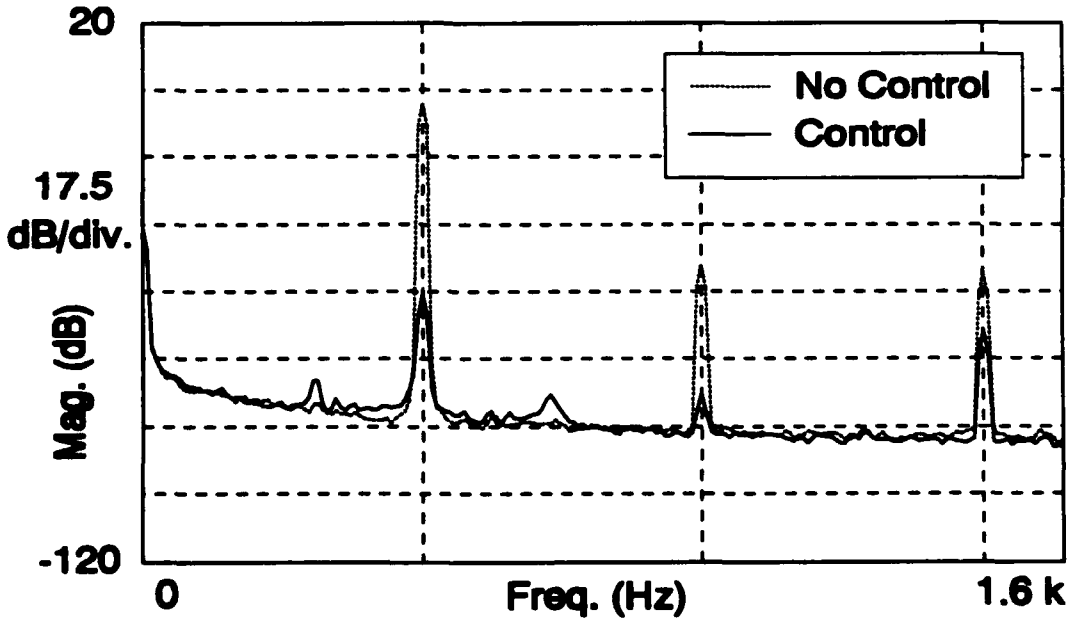

Figure 6.12 Downstream Acceleration, Acceleration Control, 488 Hz, Setup 3.

6.2.3 Intensity Control in the Nearfield

This section examines the implementation of the intensity control with the error sensor positioned relatively near to the control actuators. The theory in Section 2.2 leads one to expect that the intensity control will outperform the acceleration control for this configuration. The results obtained over the range of configurations are not conclusive, but seem to indicate that it is possible to obtain improved attenuation using intensity control.

A representative example of the adaptive control of the short error function signal is given in Figure 6.13. The error function is controlled well in most cases. The reduction is usually on the order of 40 to 50 dB. In this case, the corresponding intensity signal experiences a significant reduction. As shown in Figure 6.14, the intensity signal is reduced approximately 30 dB at the frequency $2\omega_0$, and it is reduced approximately 30 dB at the dc value. The resulting reduction of the downstream acceleration signal, shown in Figure 6.15, is on the order of 17 dB. This is compared with the downstream acceleration reduction achieved with acceleration control, shown in Figure 6.16, of approximately 10 dB. Another example of intensity control performing better than acceleration control is shown next. In Figure 6.17, the downstream acceleration signal resulting from intensity control at 340 Hz is shown. The reduction in downstream acceleration is approximately 15 dB. This is compared to the reduction in downstream acceleration resulting from acceleration control, which is shown in Figure 6.18. The reduction is approximately 5 dB.

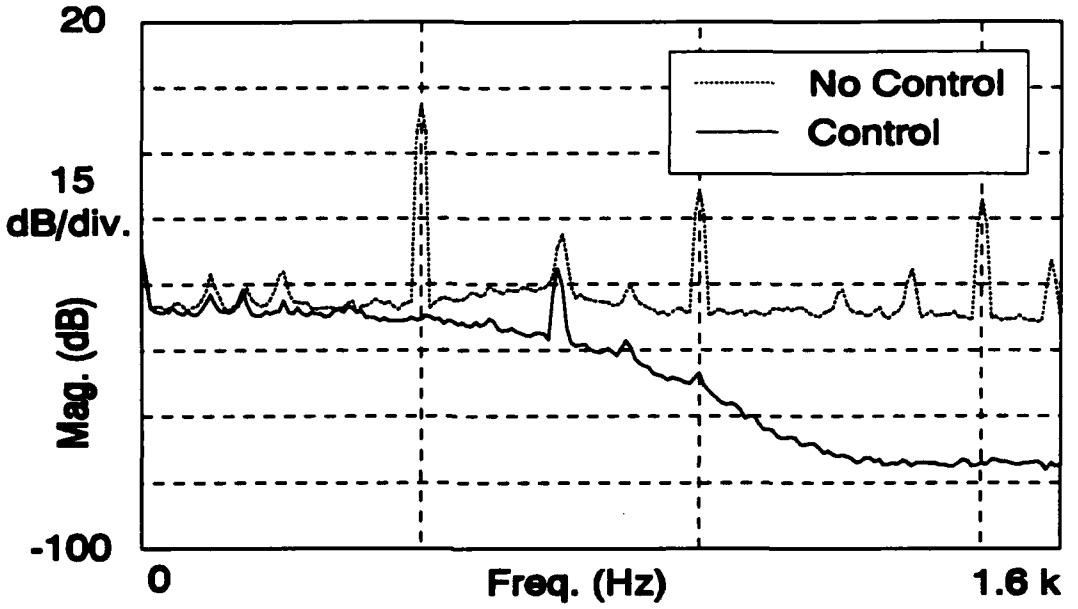

Figure 6.13 Error Function, Short Error Intensity Control, Moment Actuator, 488 Hz, Setup 2.

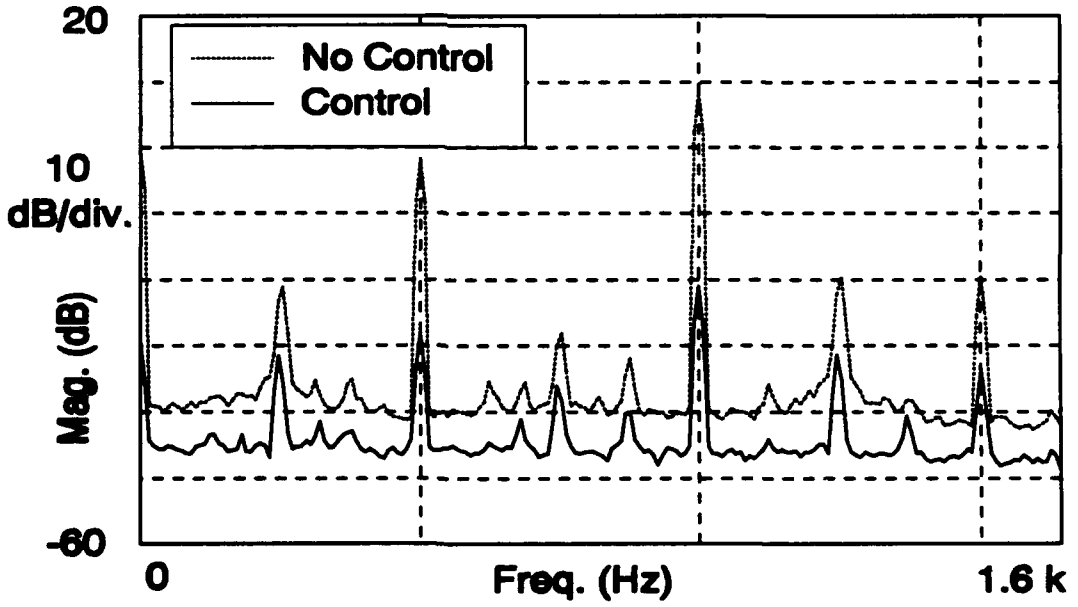

Figure 6.14 Intensity Signal, Short Error Intensity Control, Moment Actuator, 488 Hz, Setup 2.

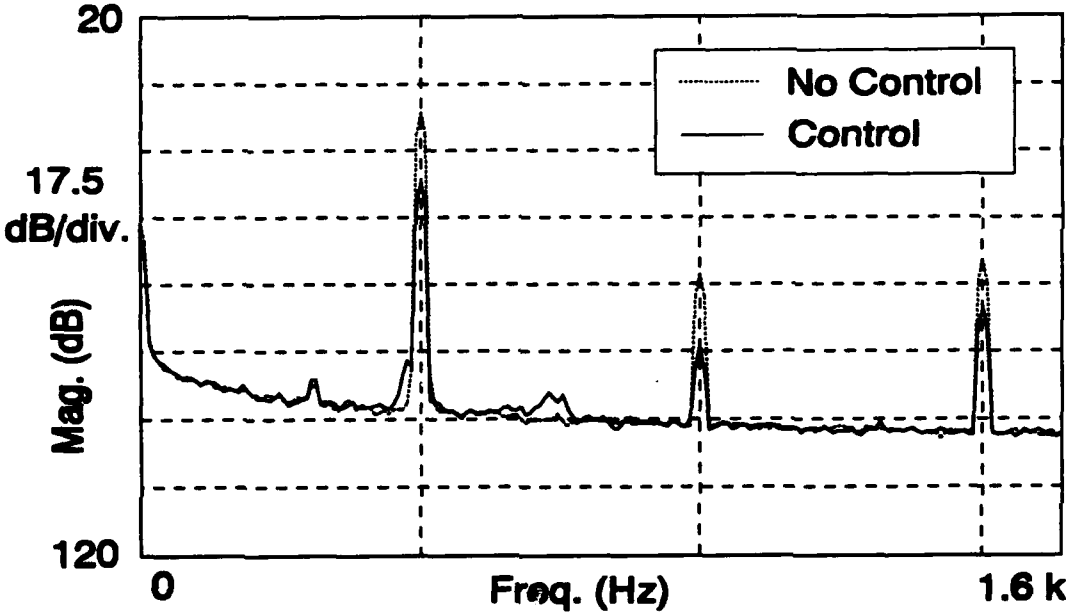

Figure 6.15 Downstream Acceleration, Short Error Intensity Control, Moment Actuator, 488 Hz, Setup 2.

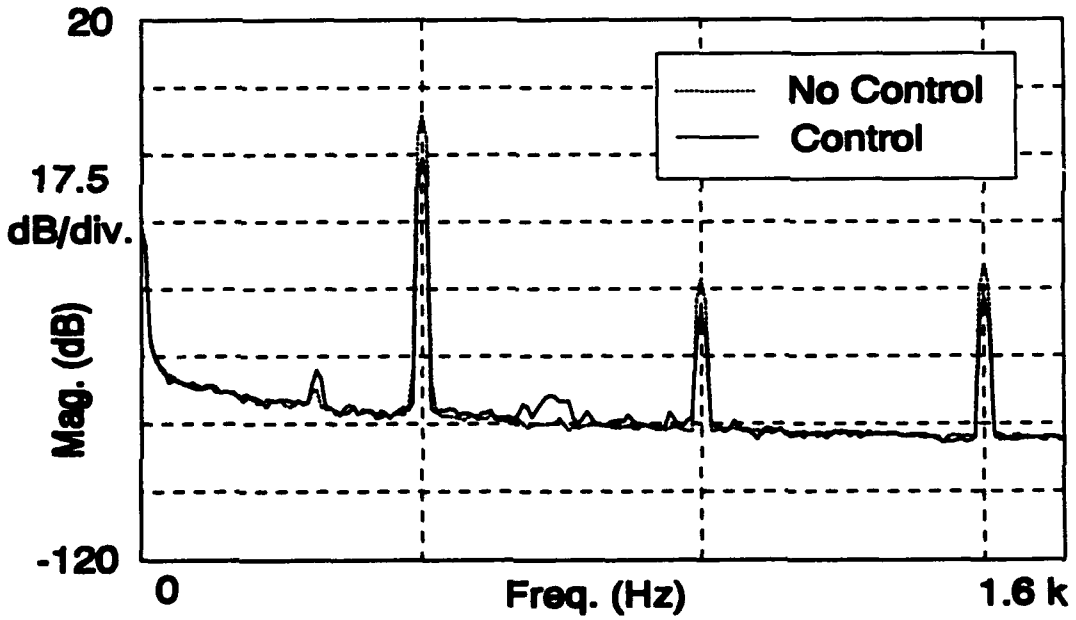

Figure 6.16 Downstream Acceleration, Acceleration Control, 488 Hz, Setup 2.

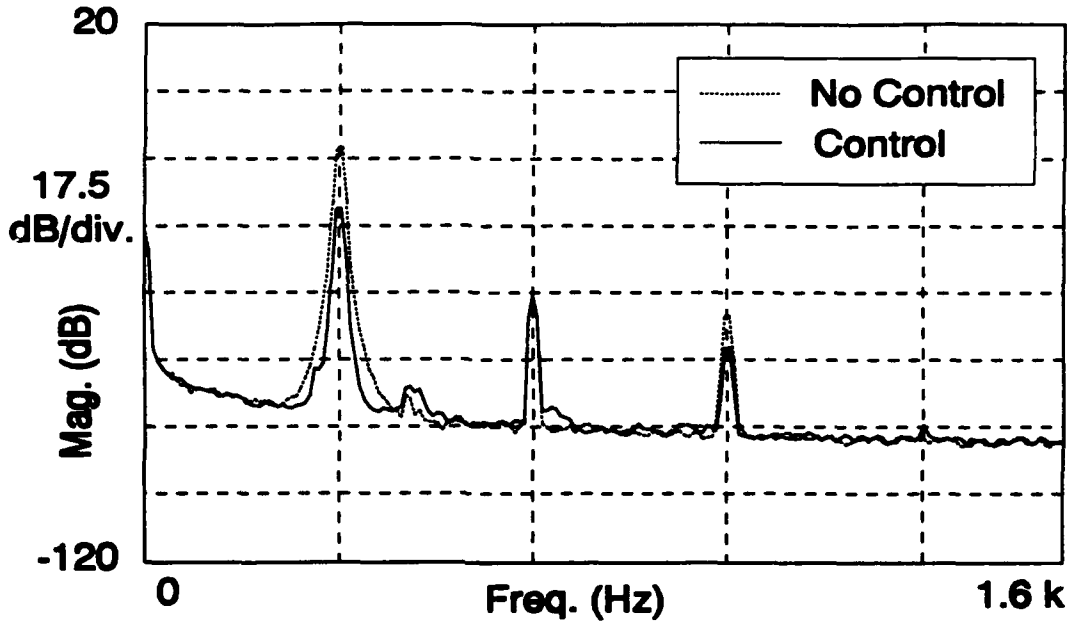

Figure 6.17 Downstream Acceleration, Short Error Intensity Control, Force and Moment Actuators, 340 Hz, Setup 2.

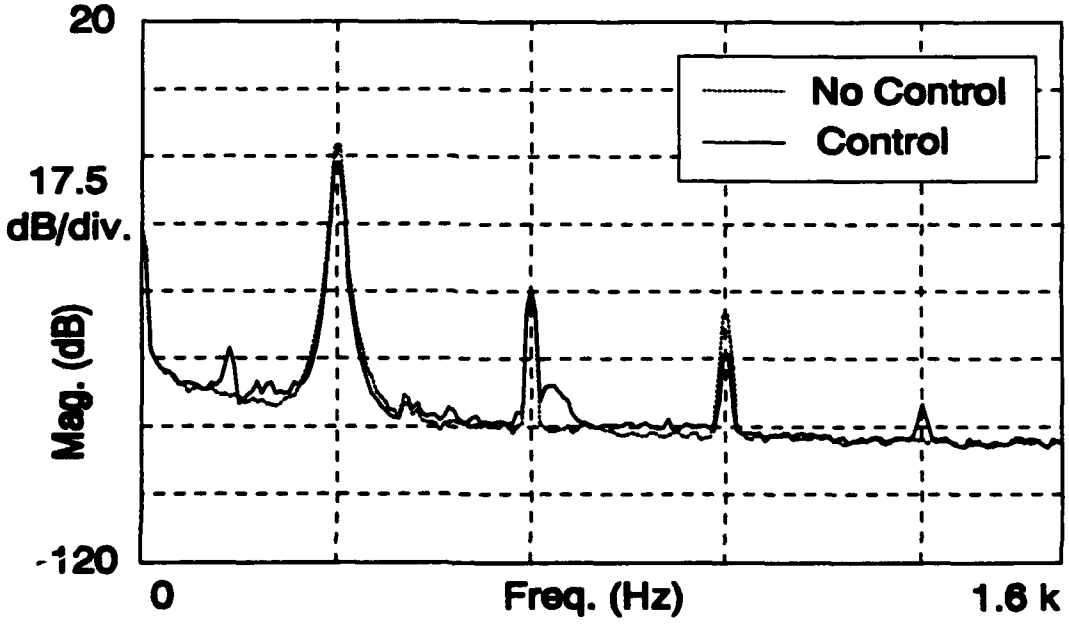

Figure 6.18 Downstream Acceleration, Acceleration Control, 340 Hz, Setup 2.

It should be noted that the cases where the intensity control outperforms the acceleration control are few. In the majority of the tests run, the intensity control falls short of the acceleration control. In performing the tests, several trends are identified which may contribute to these difficulties. Some of these trends and problems are discussed in the following sections.

6.2.4 Frequency Dependence of Intensity Control

The first problem associated with intensity control that is discussed is that of frequency dependence. The short error intensity control scheme with a force actuator only is examined at all frequencies. The control actuator is positioned near to the excitation shaker and the error sensor is positioned relatively near to the control actuators.

The control scheme works better at the higher frequencies. This seems to be true because the error function has a higher signal-to-noise ratio at these frequencies. In Figure 6.19, it can be seen that although the control reduced the error function signal to the noise floor, at the 140 Hz excitation frequency, this amounts to only a 25 dB reduction in the error function signal. This results in a small reduction in the downstream acceleration signal, as shown in Figure 6.20. Likewise, as shown in Figure 6.21 which displays control with an excitation frequency of 340 Hz, a signal-to-noise ratio for the error function signal of about 35 dB re·lts in an increase in the downstream acceleration signal, shown in Figure 6.22. However, when the signal-to-noise ratio of the error function is on the order of 45 to 50 dB, as is the case for

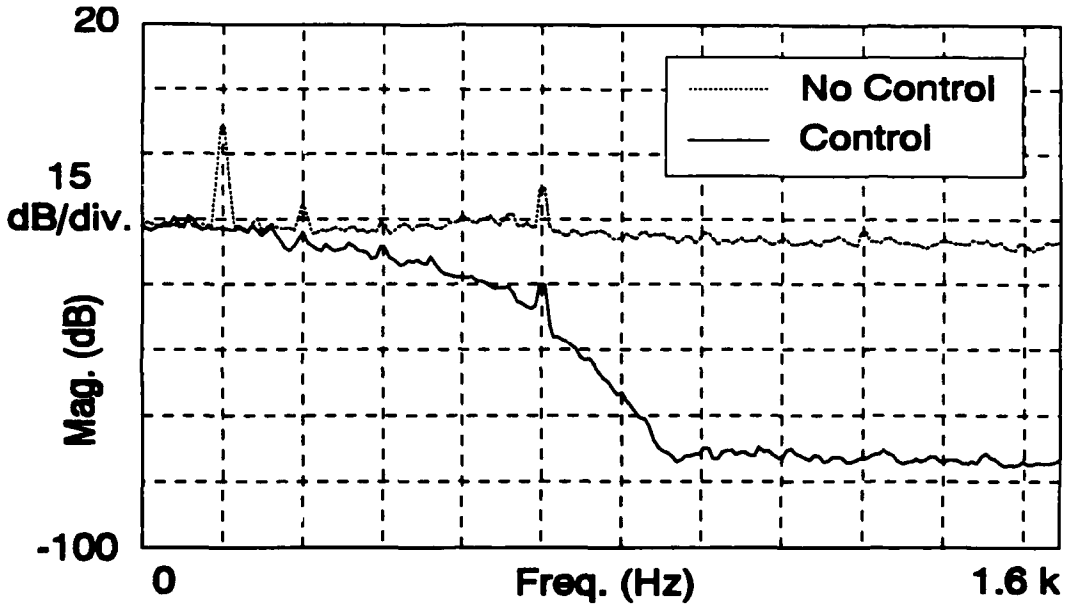

Figure 6.19 Error Function, Short Error Intensity Control, Force Actuator, 140 Hz, Setup 4.

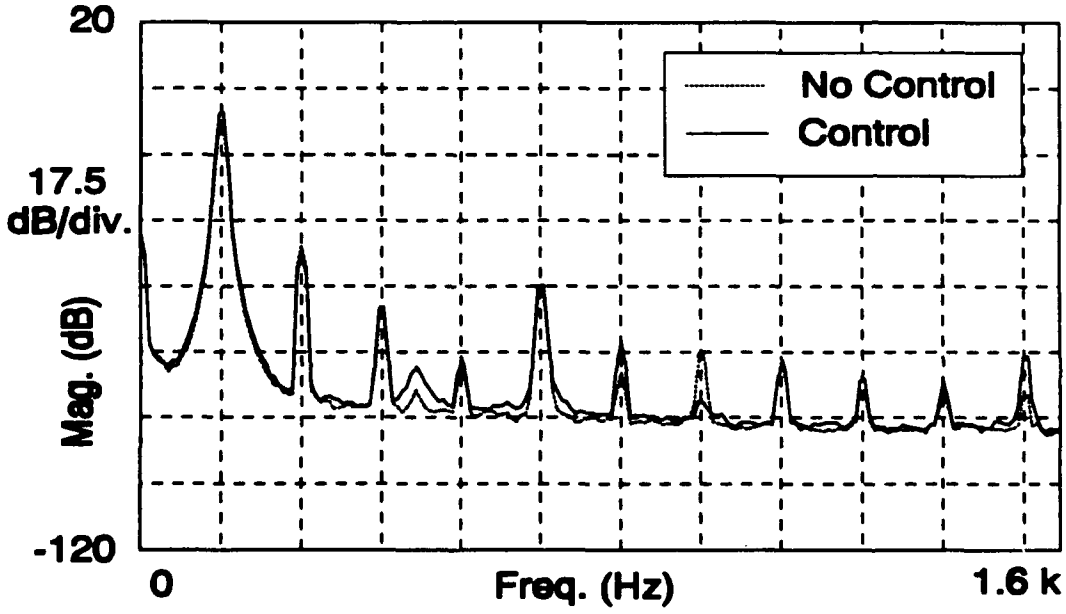

Figure 6.20 Downstream Acceleration, Short Error Intensity Control, Force Actuator, 140 Hz, Setup 4.

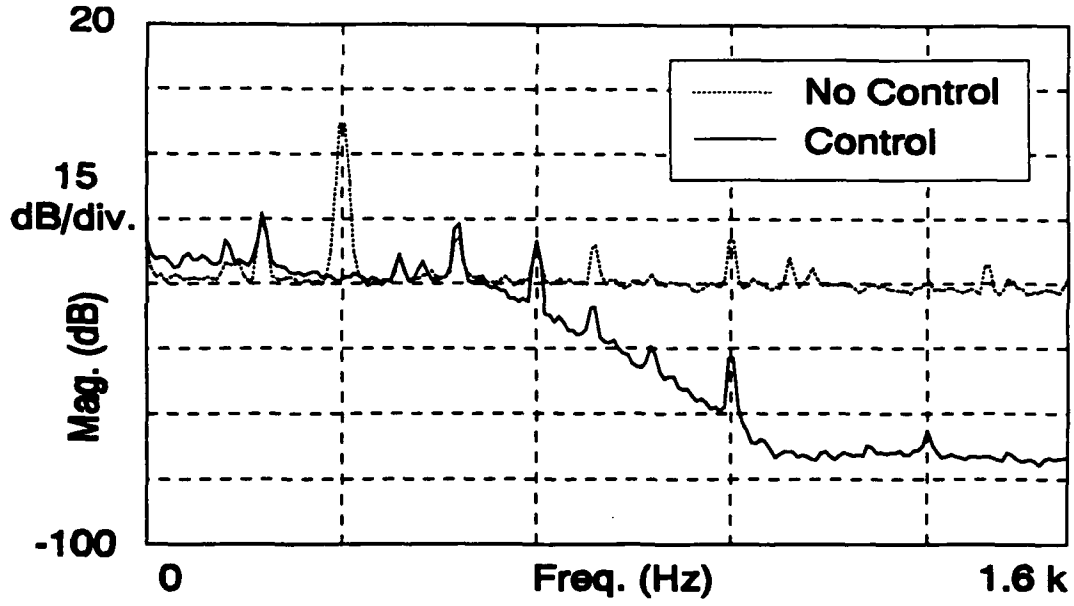

Figure 6.21 Error Function, Short Error Intensity Control, Force Actuator, 340 Hz, Setup 4.

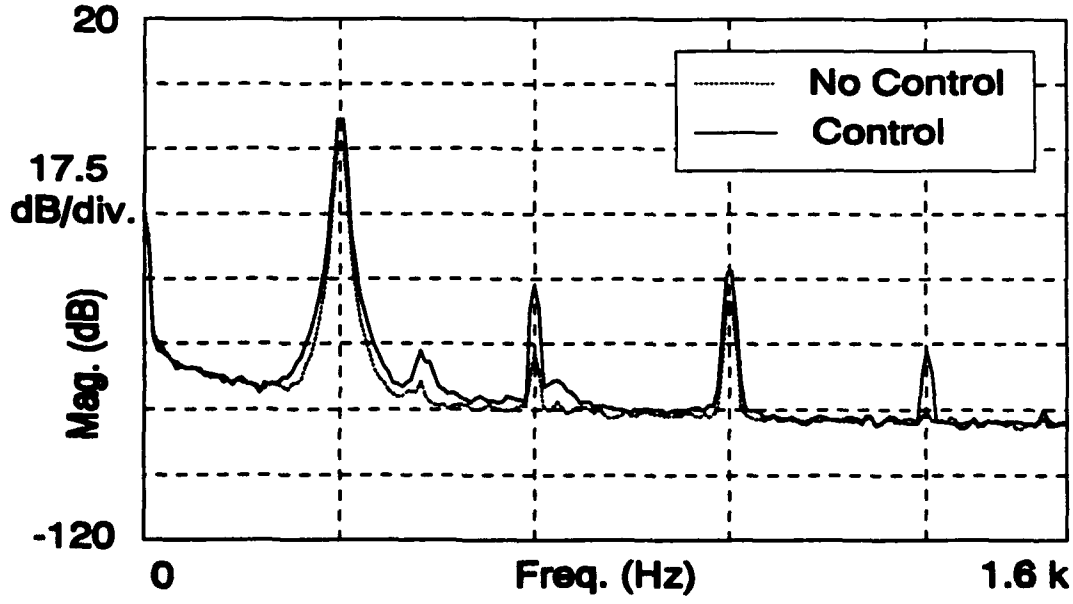

Figure 6.22 Downstream Acceleration, Short Error Intensity Control, Force Actuator, 340 Hz, Setup 4.

excitation frequencies 296, 488, and 520 Hz (see Figures 6.23, 6.24, and 6.25, respectively), the resulting reduction in the downstream acceleration signal is on the order of 10-20 dB, as shown in Figures 6.26, 6.27, and 6.28. It should be noted that at 200 Hz, the control scheme failed to converge. This strengthens the claim that the scheme works better at higher frequencies.

A possible explanation for this frequency dependence concerns the accelerometer spacing in terms of the flexural wavelength, λ. The wavelengths for the various frequencies of interest are given in Table 5.1. The spacing between accelerometers is 4 cm. At the highest frequency, 520 Hz, this corresponds to about 0.067 λ. At the lowest frequency, 140 Hz, this accelerometer spacing corresponds to about 0.034 λ. The reason the accelerometers should be spaced farther apart, relative to a wavelength, is that in the spatial finite differencing schemes neighboring acceleration values are subtracted, in order to approximate the spatial derivatives. If these signals are almost equal, more error will be introduced, with a finite bit accuracy processor, than if the signals are not almost equal. Positioning the accelerometers close, relative to a wavelength, ensures the neighboring values will be almost equal.

Another possible explanation for the frequency dependence concerns the sampling frequency versus the driving frequency. This discussion is analogous to the one for geometrical spacing given previously. The successive, in time, signals are subtracted to give an approximation of the time derivatives. The closer these signals are to being equal, the more processing error will be introduced into the derivative approximation. Sampling the signals closer, relative to driving frequency,

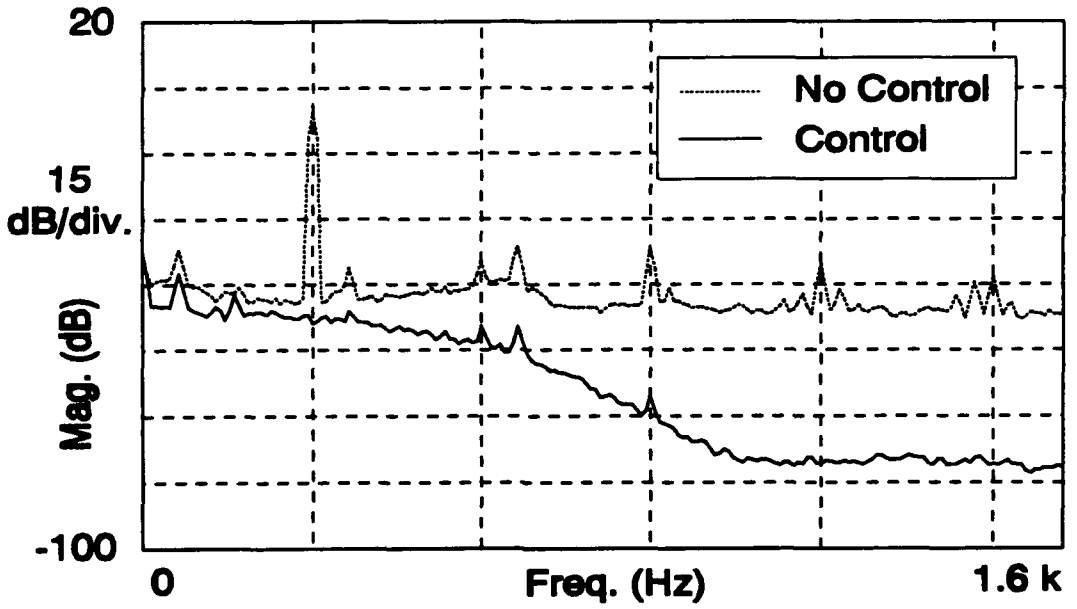

Figure 6.23 Error Function, Short Error Intensity Control, Force Actuator, 296 Hz, Setup 4.

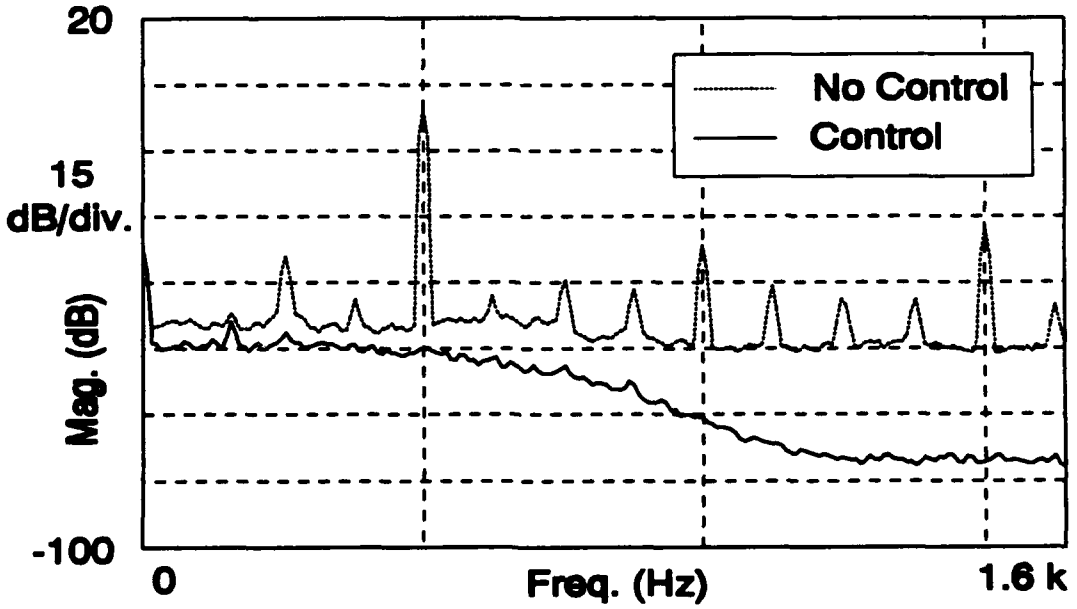

Figure 6.24 Error Function, Short Error Intensity Control, Force Actuator, 488 Hz, Setup 4.

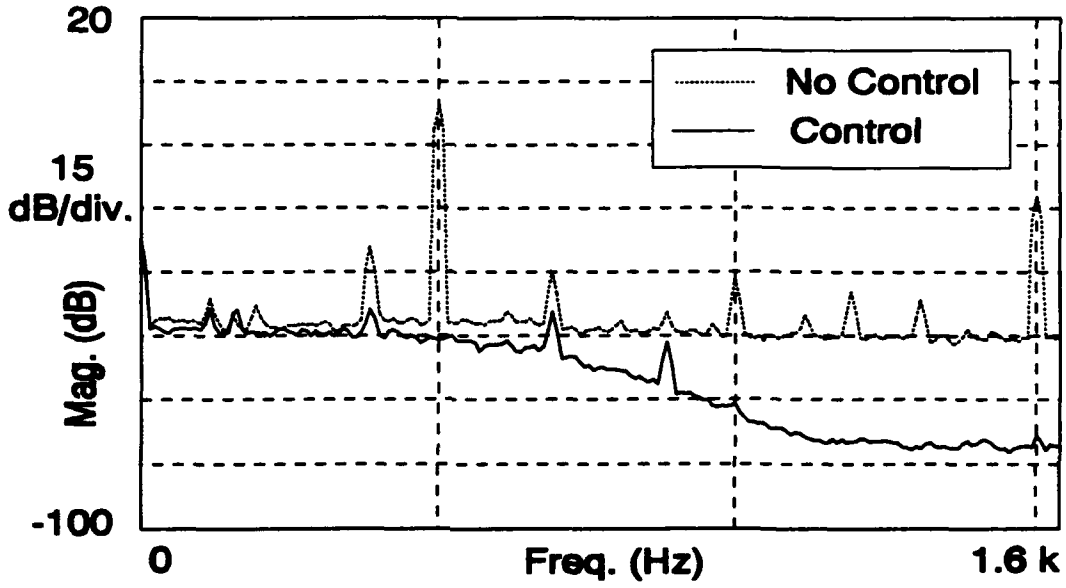

Figure 6.25 Error Function, Short Error Intensity Control, Force Actuator, 520 Hz, Setup 4.

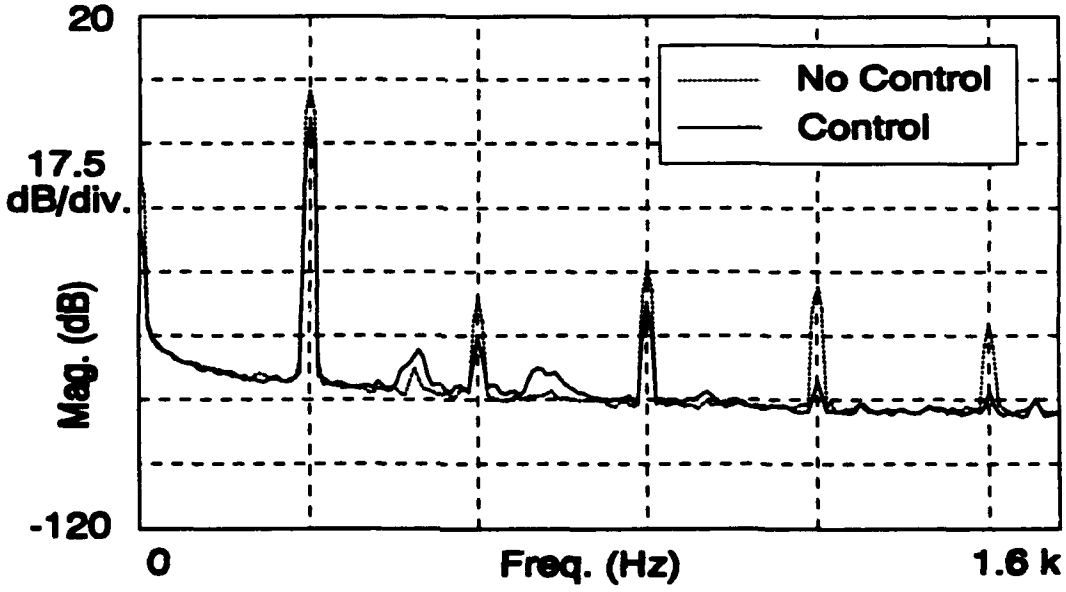

Figure 6.26 Downstream Acceleration, Short Error Intensity Control, Force Actuator, 296 Hz, Setup 4.

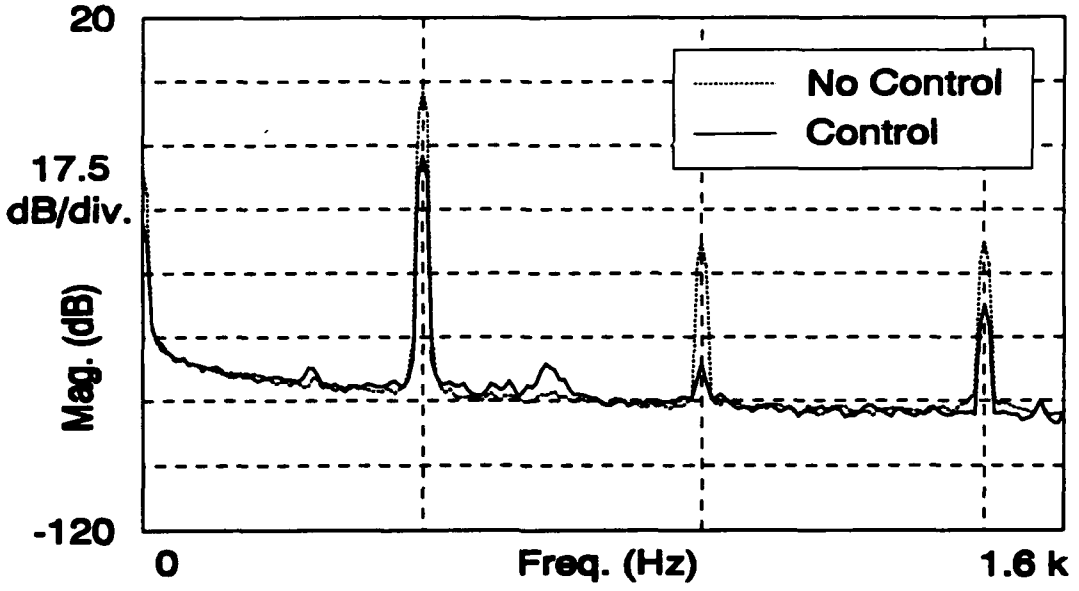

Figure 6.27 Downstream Acceleration, Short Error Intensity Control, Force Actuator, 488 Hz, Setup 4.

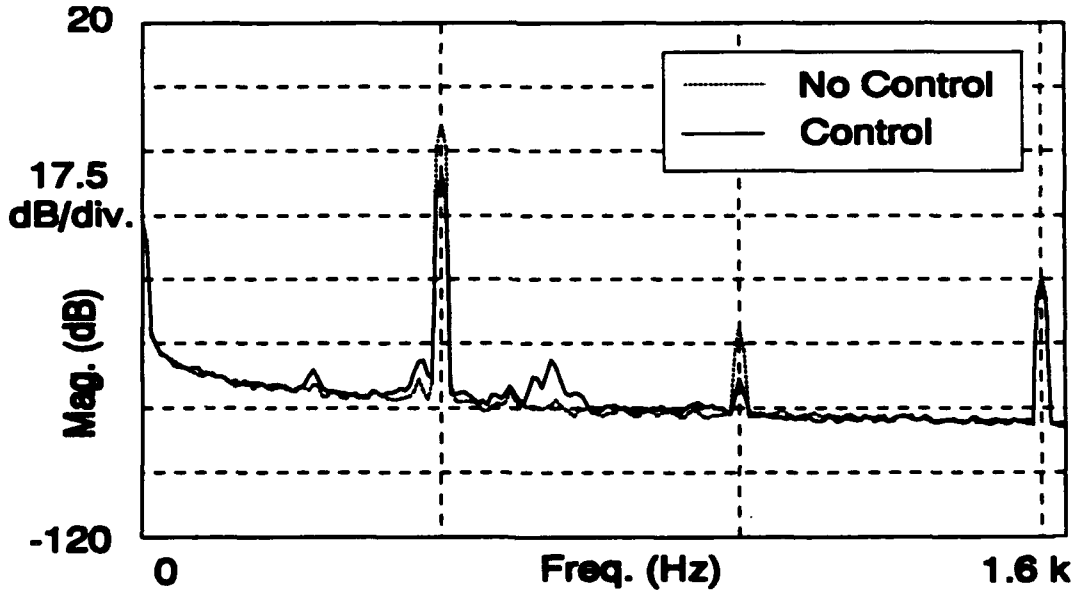

Figure 6.28 Downstream Acceleration, Short Error Intensity Control, Force Actuator, 520 Hz, Setup 4.

ensures that the successive samples are closer to being equal.

A third explanation for this frequency dependence relates the beam length to the wavelength. One should recall that a $+x$ travelling wave is assumed in the development of the intensity error functions. The wavelength at lower frequencies approaches the length of the beam. Thus, the error sensor is in a different wave field at the lower frequencies than at the higher frequencies. The more the field is dominated by waves other that $+x$ travelling waves, the more the error function is no longer valid, and the less the calculated error function relates to the true gradient of intensity.

6.2.5 Long Error Function

The next problem associated with intensity control concerns the long error function. A reduction in the long error function signal used does not necessarily result in a reduction in the intensity signal.

As is shown in Figure 6.29, the given control scheme succeeded in reducing the error function signal by approximately 55 dB. However, the intensity signal, shown in Figure 6.30, increased to the point that it exceeded the ±8.19 V limit of the output board. It should be noted that because the intensity signal is clipped, the frequency plot of Figure 6.30 is not a true representation of the signal, but it serves to express the fact that the intensity signal increased.

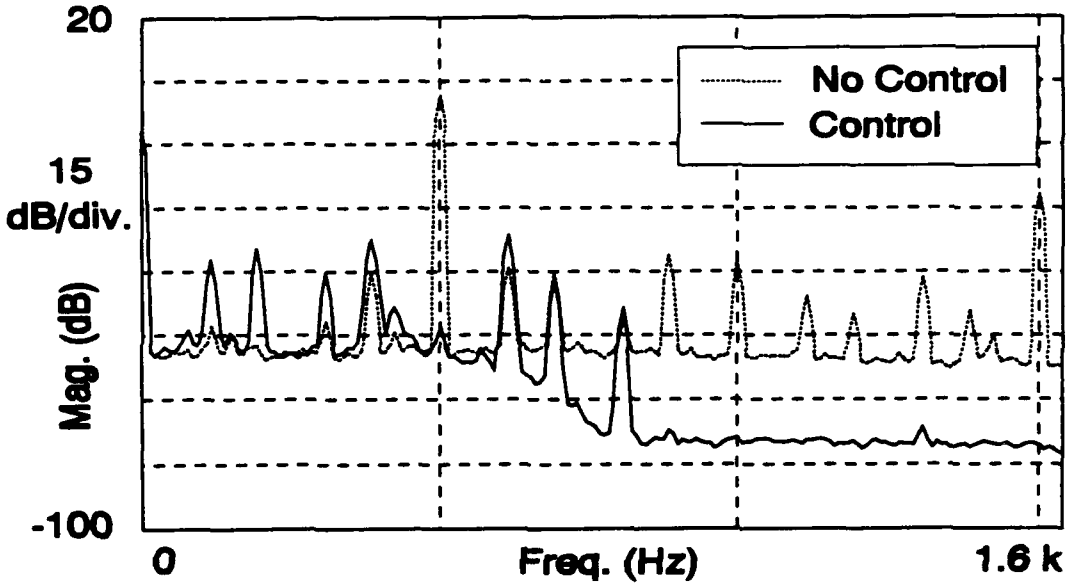

Figure 6.29 Error Function, Long Error Intensity Control, Force Actuator, 520 Hz, Setup 2.

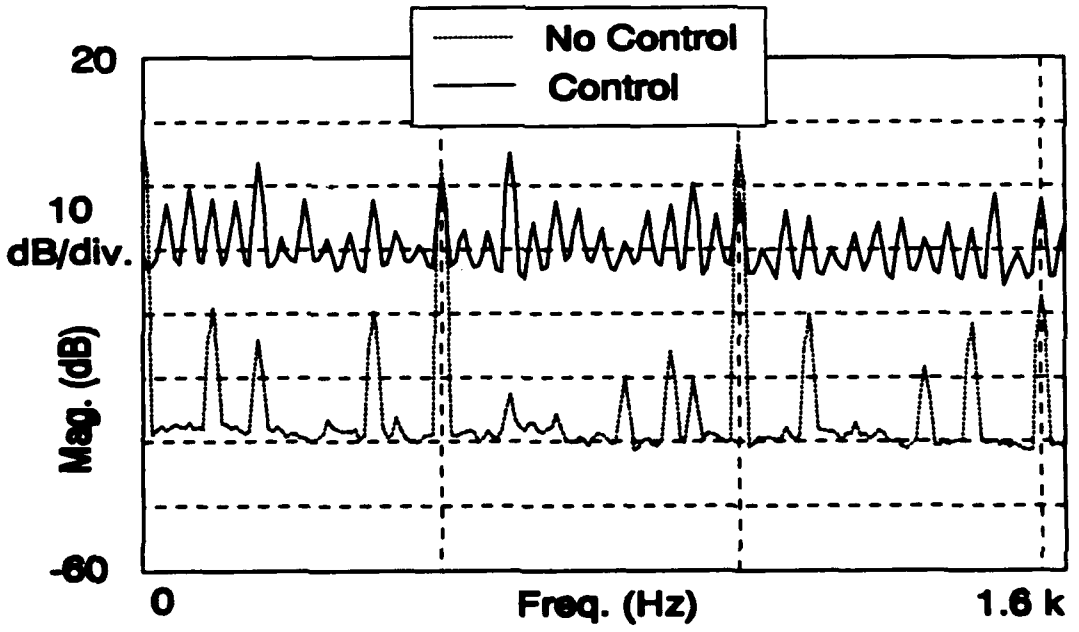

Figure 6.30 Intensity Signal, Long Error Intensity Control, Force Actuator, 520 Hz, Setup 2.

This apparent lack of correlation between the long error function and the intensity is not universal. As is shown in Figures 6.31 and 6.32, controlling the long error signal sometimes reduces the intensity.

One reason for this correlation/lack of correlation concerns the $+x$ travelling wave assumption made in estimating the gradient. If the wave field is dominated by another type of wave, the expression for the gradient does not necessarily correlate with the true gradient, and, therefore, it does not correlate with the intensity.

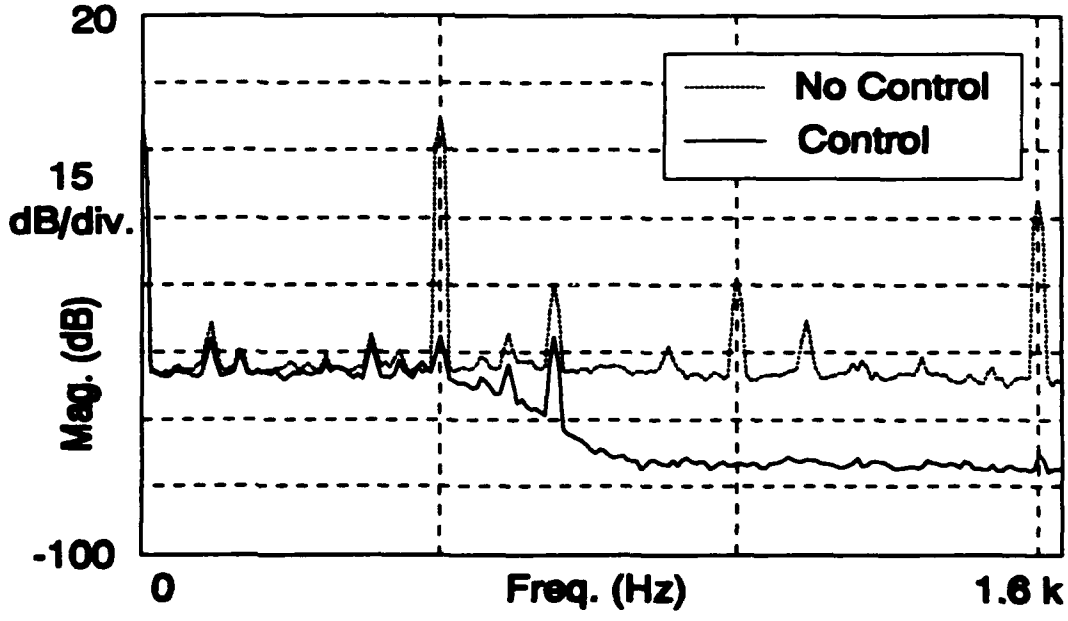

Figure 6.31 Error Function, Long Error Intensity Control, Force Actuator, 520 Hz, Setup 3.

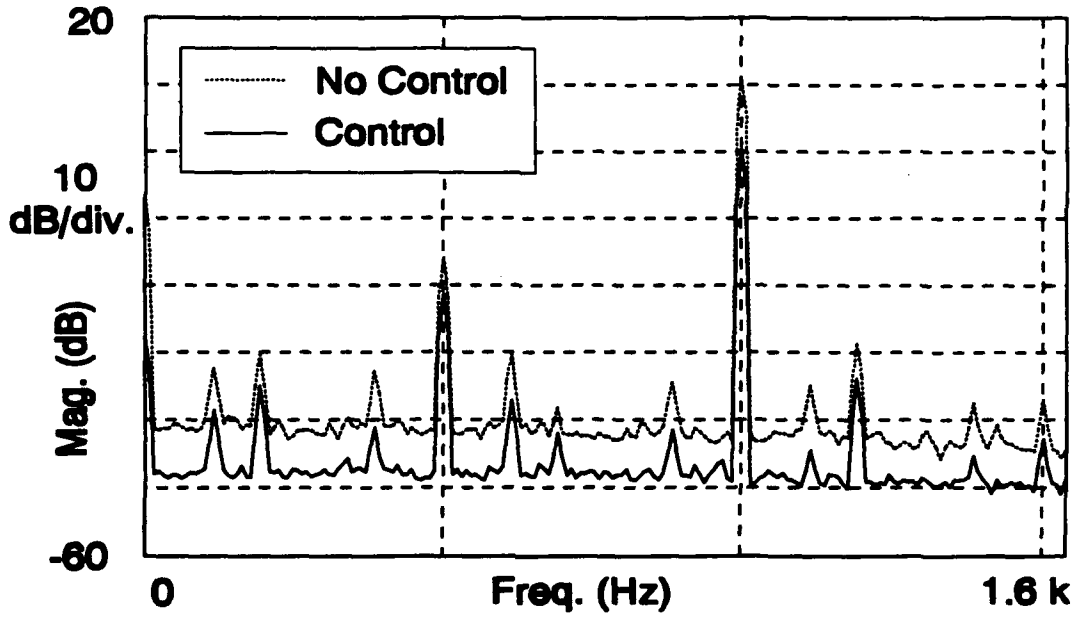

Figure 6.32 Intensity Signal, Long Error Intensity Control, Force Actuator, 520 Hz, Setup 3.

6.2.6 Short Error Function

It is found that, although the short error function seems to correlate with the intensity, there are still problems with this error function. One problem is that the error signal is too noisy at low frequencies. As can be seen in Figure 6.33, the signal-to-noise ratio of the error signal at 200 Hz for setup 1 is less than 30 dB. This noise is thought to be numerical noise resulting from the finite difference schemes.

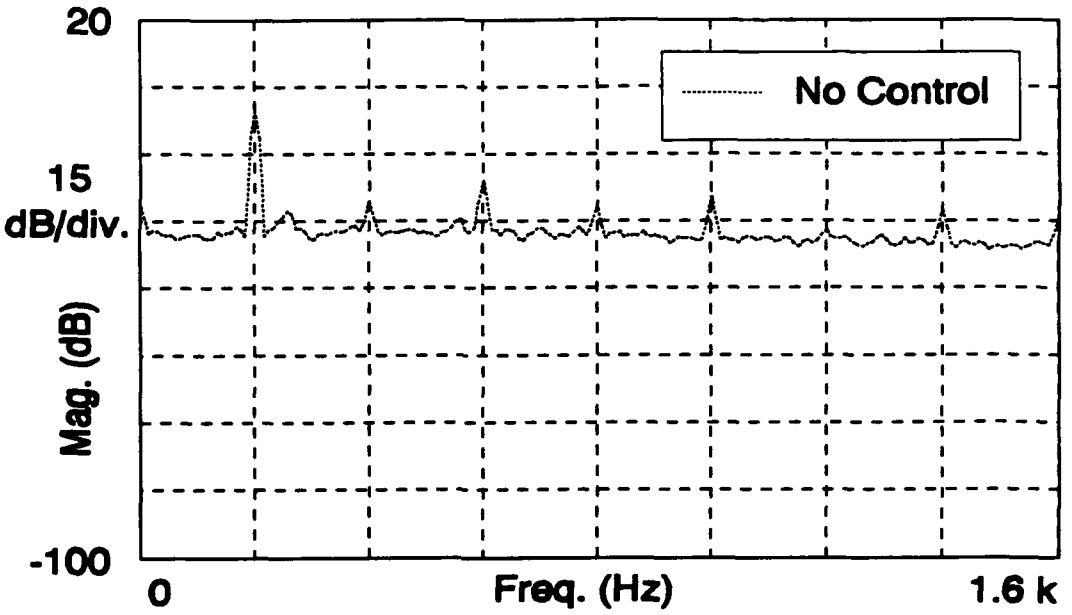

Figure 6.33 Short Error Function, No Control, 200 Hz, Setup 1.

6.2.7 Actuator Configuration Dependence

The final issue concerning intensity control to be examined is that of control actuator configuration dependence. There are no strong trends of one actuator configuration outperforming another to any great degree, but the trend appears to be that the moment actuator configuration works slightly better than the force and moment actuators configuration, which works slightly better than the force actuator configuration.

At the frequency examined, the short error function signal for each of the three configurations is reduced by similar amounts. A representative case of this is shown in Figure 6.34; the error function in all cases is reduced on the order of 45 dB.

However, the difference is found in the traces of downstream acceleration. The force actuator configuration, shown in Figure 6.35, reduces the downstream acceleration about 13 dB. The moment actuator configuration, shown in Figure 6.36, reduces the downstream acceleration by approximately 17 dB. The force and moment actuators configuration, shown in Figure 6.37, reduces the downstream acceleration slightly less--about 15 dB.

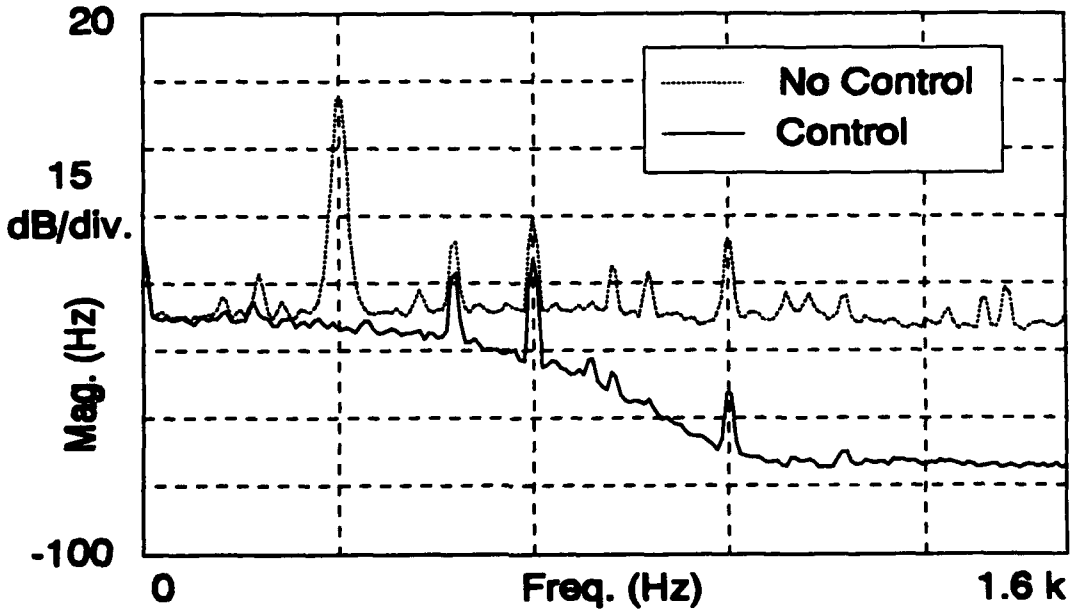

Figure 6.34 Error Function, Short Error Intensity Control, Force Actuator, 340 Hz, Setup 2.

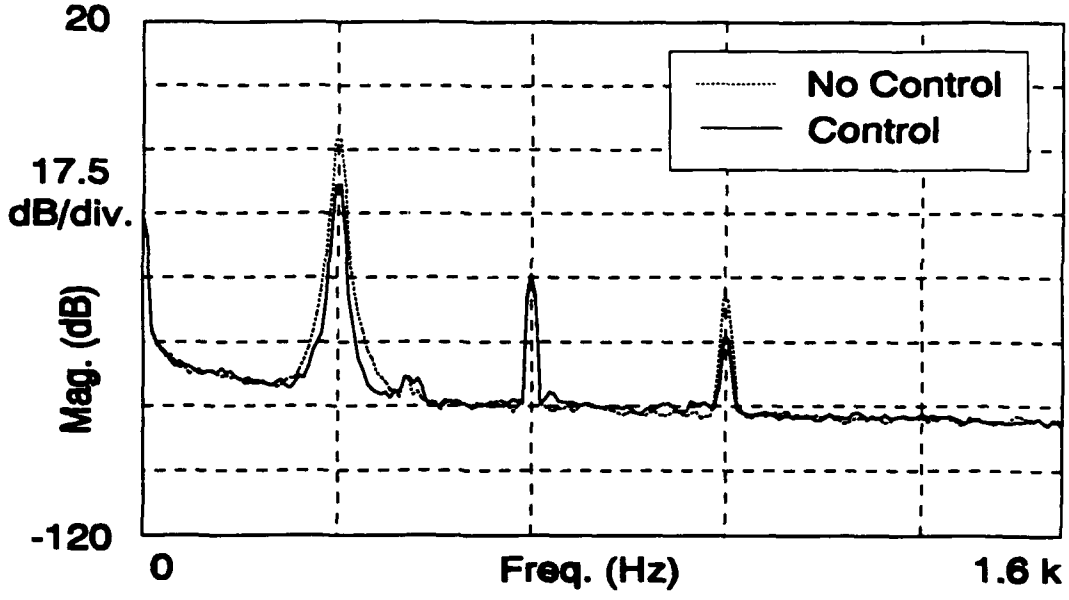

Figure 6.35 Downstream Acceleration, Short Error Intensity Control, Force Actuator, 340 Hz, Setup 2.

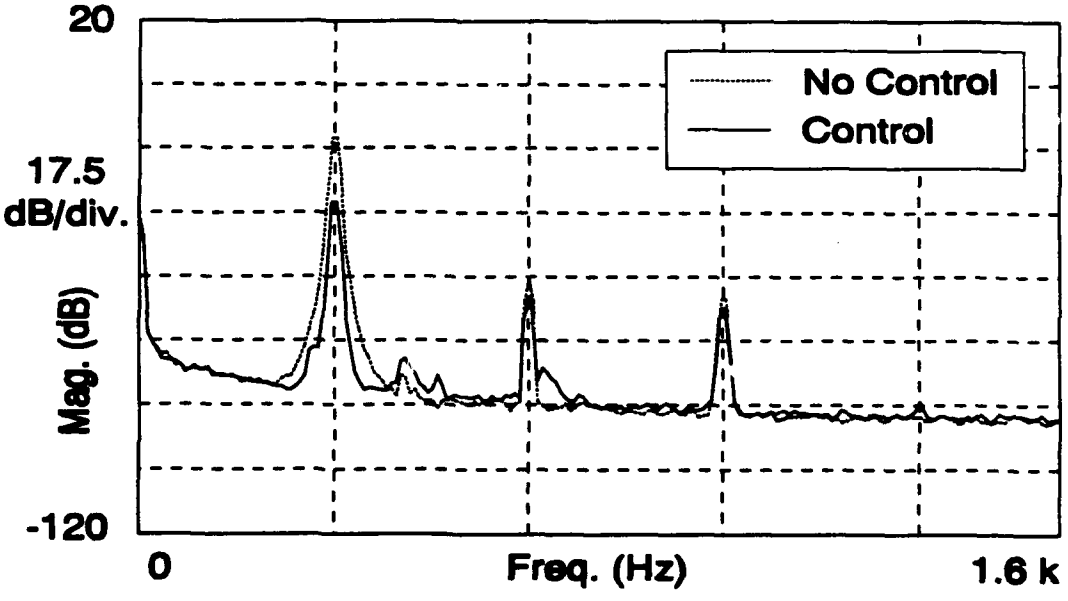

Figure 6.36 Downstream Acceleration, Short Error Intensity Control, Moment Actuator, 340 Hz, Setup 2.

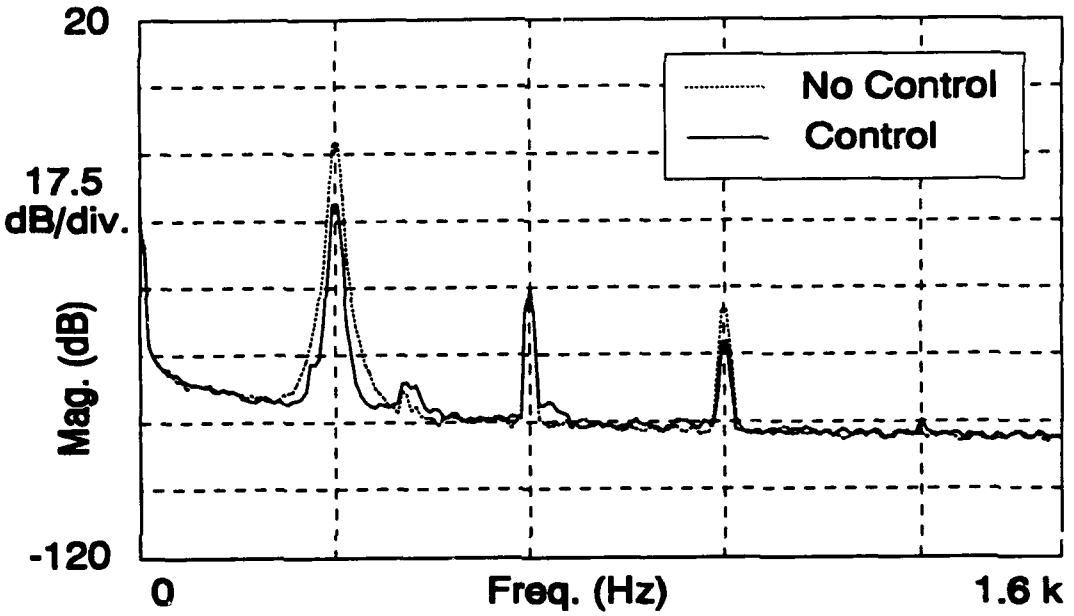

Figure 6.37 Downstream Acceleration, Short Error Intensity Control, Force and Moment Actuators, 340 Hz, Setup 2.

Chapter 7

CONCLUSIONS AND RECOMMENDATIONS

In this chapter, Section 7.1 examines the conclusions of the research, and Section 7.2 recommends several possible areas for future research.

7.1 Conclusions

The goals of this thesis were to develop, implement, and evaluate several algorithms for the adaptive vibration control of the total, instantaneous structural intensity in a beam. A measurement algorithm based on finite difference schemes was developed for calculating the necessary partial derivatives in both space and time. A control algorithm based on the filtered-x algorithm was developed. The intensity control algorithm used one of two derived error functions and one of three actuator configurations to implement the control of structural intensity. The various intensity control schemes were evaluated relative to acceleration control by means of a downstream acceleration signal. Evaluation of the results from these tests led to several conclusions.

The first conclusion is that acceleration control was more effective with the error sensor in the farfield than in the nearfield, which was predicted in Section 2.2.

Furthermore, with the error sensors positioned relatively far from the control actuators, controlling acceleration was more effective than controlling intensity, using the algorithms developed in this study. Although the theory predicts that the two

schemes will perform equally well, noise in the error signal degrades the effectiveness of the control algorithm, when controlling intensity.

In addition, with the error sensors positioned relatively near to the control actuators, the attenuation achieved by controlling intensity was comparable to or greater than that achieved by controlling acceleration. It was predicted that this attenuation should always be greater when controlling intensity than when controlling acceleration. The reasons for this discrepancy include frequency dependence of the control schemes and numerical noise in the computation of the error function signals.

The performance of the intensity control schemes is frequency dependent due to the frequency dependence of the numerical noise introduced by the finite difference schemes. In addition, the beam length relative to the flexural wavelength of vibration at low frequencies places the error sensor in a wave field dominated by waves other than the assumed $+x$ travelling waves.

The performance of the intensity control schemes is strongly dependent upon the choice of error function. The long error function frequently does not give a true representation of the gradient of intensity. This is due to the assumption that the wave field is dominated by $+x$ travelling waves which is not valid in the nearfield.

Signal noise was a problem at all frequencies, with both gradient approximations. This noise consists of electronic noise from the accelerometers and numerical noise from the finite difference techniques.

The performance of the intensity control schemes does not seem to depend upon the actuator configuration. The three configurations, force only, moment only,

and force and moment, all result in similar reductions in both the error function signal and the downstream acceleration signal.

7.2 Recommendations for Further Research

Based upon the results of this study and the above conclusions, several recommendations for future research are made. These should include a more in-depth study of the intensity measurement, including the gradient of intensity, developing the control algorithms to be able to discriminate between active and reactive intensity, and increasing the complexity of the structure being controlled.

A different method for calculating the intensity will be needed if control of broadband vibrations is to be achieved. The method described in this thesis used a multiplication by $-1/\omega_0^2$ to achieve double integration in time, which assumes single frequency excitation at a known frequency, ω_0. One alternative would be to investigate using piezoelectric strain gauges. These strain gauges would allow a measure of strain, which may lead to an improved intensity estimate capable of making broadband intensity measurements. Another alternative would be to pass the acceleration signals through linear analog integrators, designed to be effective over the frequency range of interest. Using transducer combinations, such as both strain gauges and accelerometers, should also be considered.

It should be noted that any multiple frequency study would necessitate a broadband calibration of the transducers. Currently, the control schemes use a single

calibration constant for each accelerometer at the excitation frequency. Perhaps a frequency domain calibration could be performed using a FIR filter approximation.

Another quantity that warrants further investigation is the estimate of the gradient of the intensity. At times, a substantial reduction in the long error signal used in this study did not result in any reduction in the intensity. A reevaluation of the assumptions will be necessary in order to hopefully develop a more valid expression for the gradient of intensity.

An additional area to investigate is the separation of the active and the reactive intensity. Because the active intensity represents the energy which propagates to the farfield, it would often be desirable to control just the active intensity.

A final recommendation is to extend the method of controlling intensity to more complex structures. For one-dimensional structures, this could include different terminations, terminations at both ends, and coupled beams with various joints. The study could also be implemented on two-dimensional structures, such as plates and shells.

REFERENCES

[1] R. F. Drenick and R. A. Shahbender, "Adaptive Servo-mechanisms," *Applications and Industry*, Nov. 1957, pp. 286-292.

[2] P. R. Stromer, "Adaptive or Self-Optimizing Control Systems--A Bibliography," *IRE Transactions on Automatic Control*, Vol. AC-4, No. 1, May 1959, pp. 65-68.

[3] G. W. Anderson, J. A. Aseltine, A. R. Mancini, and C. W. Sarture, "A Self-Adjusting System for Optimum Dynamic Performance," *IRE National Convention Record*, Part 4, 1958, pp. 182-190.

[4] H. L. Groginsky, "On the Design of Adaptive Systems," *IRE National Convention Record*, Part 4, 1958, pp. 160-167.

[5] H. F. Olson, "Electronic Control of Noise, Vibration, and Reverberation," *J. Acoust. Soc. Am.*, Vol. 28, No. 5, Sept. 1956, pp. 966-972.

[6] J. A. Bonesho and J. G. Bollinger, "How to Design a Self-Optimizing Vibration Damper," *Machine Design*, Vol. 40, No. 5, Feb. 29, 1968, pp. 123-127.

[7] C. E. Kaplow and J. R. Velman, "Active Local Vibration Isolation Applied to a Flexible Space Telescope," *J. Guidance and Control*, Vol. 3, No. 3, May-June 1980, pp. 227-233.

[8] T. Bailey and J. E. Hubbard Jr., "Distributed Piezoelectric-Polymer Active Vibration Control of a Cantilever Beam," *J. Guidance*, Vol. 8, No. 5, Sept.-Oct. 1985, pp. 605-611.

[9] C. R. Johnson Jr., "Adaptive Modal Control of Large Flexible Spacecraft," *J. Guidance and Control*, Vol. 3, No. 4, July-August 1980, pp. 369-375.

[10] H. Öz and L. Meirovitch, "Optimal Modal-Space Control of Flexible Gyroscopic Systems," *J. Guidance and Control*, Vol. 3, No. 3, pp. 218-226.

[11] B. Widrow and S. D. Stearns, *Adaptive Signal Processing*, Englewood Cliffs, NJ: Prentice-Hall, 1985.

[12] S. D. Sommerfeldt and J. Tichy, "Adaptive Control of a Two-Stage Vibration Isolation Mount," *J. Acoust. Soc. Am.*, Vol. 88, No. 2, August 1990, pp. 938-944.

[13] S. D. Sommerfeldt, "Multi-channel Adaptive Control of Structural Vibration," *Noise Control Engineering Journal*, Vol. 37, No. 2, Sept.-Oct. 1991, pp. 77-89.

[14] S. D. Sommerfeldt and P. J. Nashif, "Energy Based Control of the Sound Field in Enclosures," to appear in *Proceedings of the Second International Congress on Recent Developments in Air- & Structure-Borne Sound and Vibration*, Auburn, AL, March 1992, pp. 361-368.

[15] D. U. Noiseux, "Measurement of Power Flow in Uniform Beams and Plates," *J. Acoust. Soc. Am.*, Vol. 47, No. 1 (Part 2), 1970, pp. 238-247.

[16] G. Pavic, "Measurement of Structure Borne Wave Intensity, Part I: Formulation of the Methods," *Journal of Sound and Vibration*, Vol. 49, No. 2, 1976, pp. 221-230.

[17] B. C. T. Suen, "Measurement and Analysis of Nearfield and Farfield Structural Intensity by Scanning Laser Vibrometry" (M.S. Thesis, The Pennsylvania State University, University Park, PA, 1990).

[18] W. Redman-White, P. A. Nelson, and A. R. D. Curtis, "Experiments on the Active Control of Flexural Wave Power Flow," *Journal of Sound and Vibration*, Vol. 112, No. 1, 1987, pp. 187-191.

[19] J. Pan and C. H. Hansen, "Active Control of Total Vibratory Power Flow in a Beam. I: Physical System Analysis," *J. Acoust. Soc. Am.*, Vol. 89, No. 1, January 1991, pp. 200-209.

[20] T. Hodges, P. A. Nelson, and S. J. Elliott, "The Design of a Precision Digital Integrator for Use in an Active Vibration Control System," *Mechanical Systems and Signal Processing*, Vol. 4, No. 4, 1990, pp. 345-353.

[21] S. D. Sommerfeldt, "Adaptive Vibration Control of Vibration Isolation Mounts, Using an LMS-Based Control Algorithm" (Ph.D. Dissertation, The Pennsylvania State University, University Park, PA, 1989).

[22] G. C. Goodwin and K. S. Sin, *Adaptive Filtering Prediction and Control*, Englewood Cliffs, NJ: Prentice-Hall, 1984.

[23] S. H. Tousi, "Complex Impedances of Structural Terminations" (B.S. Thesis, The Pennsylvania State University, University Park, PA, 1991).

[24] Spectrum Signal Processing Inc., *32 Channel Analog Input Board: User's Manual*, Waltham, MA: Spectrum Signal Processing, 1988.

[25] Spectrum Signal Processing Inc., *16 Channel Analog Output Card: User's Manual*, Westborough, MA: Spectrum Signal Processing, 1988.

[26] A. V. Oppenheim and R. W. Schafer, *Discrete-Time Signal Processing*, Englewood Cliffs, NJ: Prentice-Hall, 1989.

Appendix

ACCELEROMETER CALIBRATION CONSTANTS

Table A.1 Calibration Constants for Error Array.

Freq. (Hz)	Ser.# 1136	Ser.# 1140	Ser.# 1141	Ser.# 1142	Ser.# 1156
120	1.0000	0.8977	0.9270	1.850	1.229
140	1.0000	0.8747	0.9072	1.662	1.245
160	1.0000	0.8243	0.8860	1.493	1.261
180	1.0000	0.8276	0.8638	1.371	1.274
200	1.0000	0.8050	0.8412	1.285	1.281
220	1.0000	0.7842	0.8187	1.217	1.279
240	1.0000	0.7656	0.7969	1.156	1.266
260	1.0000	0.7494	0.7758	1.094	1.241
280	1.0000	0.7363	0.7560	1.037	1.209
300	1.0000	0.7260	0.7379	0.9897	1.175
320	1.0000	0.7186	0.7218	0.9545	1.138
340	1.0000	0.7143	0.7080	0.9295	1.107
360	1.0000	0.7120	0.6959	0.9107	1.080
380	1.0000	0.7113	0.6858	0.8925	1.060
400	1.0000	0.7124	0.6776	0.8724	1.044
420	1.0000	0.7141	0.6705	0.8502	1.034
440	1.0000	0.7164	0.6645	0.8275	1.028
460	1.0000	0.7189	0.6591	0.8044	1.026
480	1.0000	0.7217	0.6550	0.7792	1.027
500	1.0000	0.7238	0.6510	0.7433	1.031
520	1.0000	0.7261	0.6474	0.6930	1.038